On the phosphorus evaporation from liquid silicon by Knudsen effusion mass spectrometry

Arman Hoseinpur a,*, Dmitry Sergeev b, Michael Müller b, Jafar Safarian a

- a. Department of Materials science and Engineering, Norwegian University of Science and Technology (NTNU), Trondheim 7034, Norway
- b. Institute of Energy- and Climate Research–IEK 2, Forschungszentrum Jülich GmbH, Wilhelm-Johnen-Straße, 52428 Jülich, Germany
- *Corresponding author's E-mail: arman.h.kermani@ntnu.no, Phone: +47 925 08 688

Abstract

The gaseous species evaporating from the dilute liquid solutions of phosphorus in silicon were studied experimentally and it was shown that phosphorus is evaporated in form of P, P₂, P₄, P₃, SiP, Si₂P, Si₃P, and SiP₂ at elevated temperatures. Except P and P₂, the other molecules were detected experimentally for the first time, and Si₃P was detected as a new compound in the gas phase. Knudsen Effusion Mass Spectrometry technique was applied to characterize the evaporation of phosphorus from liquid Si samples containing 100, 1250, and 3000 ppmw phosphorus. The evaporation of phosphorus from liquid Si was studied by isothermal and polythermal experiments, up to 1840 °C. The vapor pressures of various P – containing molecules (P, P₂, P₄, SiP, Si₂P) at 1442 °C were measured as a function of phosphorus fraction in liquid silicon. Results indicated that a major part of the phosphorus evaporates in the form of silicon phosphides and P₄, especially when the sample temperature exceeds 1750 °C. When initial phosphorus was 100 ppmw, about 71 % of phosphorus evaporation was by means of silicon phosphides and P₄. The mechanisms of phosphorus evaporation from liquid Si are proposed, which depend on the melt composition and temperature. It occurs through phosphorus species evaporation independently or via the decomposition of transient silicon phosphides at the surface, or through the direct evaporation of silicon phosphides at the melt surface.

Keywords: Silicon phosphides, vacuum evaporation, KEMS, Phosphorus, Solar grade silicon.

1 Introduction

Silicon refining for production of Si solar cells is a hot topic attracted many researchers in recent years. The solar grade silicon (SoG - Si) requires a minimum purity of 99.9999 % (6N) [1-5] and hence dedicated refining methods are required for removing these impurities. One of the most important impurities that is difficult to remove from Si from metallurgical Si (with tens of ppmw) is phosphorus. Therefore dedicated refining techniques are required for refining of Si from P [6-15], as it is not

effectively removed via directional solidification of ingot casting. On the other hand, phosphorus is also one of the most detrimental impurities that can affect the efficiency of silicon solar cells [16]. Currently more than 90 % of the photovoltaics (PV) solar modules are produced from silicon [16-18]. and production of PV modules is increasing, as it expanded 7 folds from 2010 to 2019 [19]. Therefore, developing new processes with proper control of phosphorus in SoG – Si is important [20]. Nowadays, up to 0.2 ppmw of phosphorus in Si is accepted as the limit for SoG – Si production, which could be reduced in the future if higher efficiencies are required [21]. A lot of research works are carried out in the recent years on removal of P from Si [9,22-31] and many of them were focused on vacuum refining [1,4,5,13,32-40]. According to literature and our previous works, vacuum refining of Si is one of the most efficient and clean methods for the complete removal of phosphorus from Si [41-43]. Vacuum refining of Si has been investigated over the past 30 years and recently pilot tested/industrialized by Ferroglobe® [1,44]. The vacuum evaporation from free surfaces is called Langmuir evaporation [6,13,45-^{48]}, and hence all the research carried out for vacuum refining of Si lays in this category. Vacuum evaporation can also be studied by Knudsen technique [49] where the liquid evaporates in a tiny enclosure (cell) with an orifice on top providing a molecular beam effusing out of the cell. This beam can be characterized by spectrometers to track the evaporated molecules. Such a combination is called Knudsen Effusion Mass Spectrometry (KEMS) [50-54] , which provides valuable data about high temperature gases and vapor pressure measurements of metals and alloys [52,55-63]. Metallurgy of Si – P system is difficult to study due to high vapor pressure of P at high temperatures, requirement of dedicated instruments, and uncertainties about the gaseous species and compositions. The known gaseous components in Si – P system and at elevated temperatures are P and P₂, however, the presence of SiP, Si₂P, and Si₂P₂ has been claimed from theoretical models ^[64]. Both, thermodynamics of liquid Si – P system and the mass transport of the species between liquid and gas are reported in literature [65-68]. The thermochemistry of dilute solutions of phosphorus in Si melt has already been investigated experimentally by Miki et al. [65] and Zaitsev et al. [66], and it is theoretically modeled by Liang and Fetzer in [64]. Table 1 gives a summary of these researches. Miki et al. [65] investigated the established equilibrium of Si melt with introduced phosphorus gas in graphite and alumina crucibles and obtained the Gibbs free energy change for the equilibrium between the dissolved phosphorus in liquid Si (P) and P_{2(g)}. Zaitsev et al. [66] applied the Knudsen Effusion Mass Spectrometry method (KEMS) to investigate the vapor pressure of phosphorus species effusing from Si – P samples with various concentrations of phosphorus in liquid Si and obtained the Gibbs free energy for the evaporation of P_{2(g)} from Si melt. In the previous researches on vacuum refining of silicon [43,69] were focused on the mass transport of impurities. It has been shown that chemical evaporation at the melt surface and gas phase mass transport could control the kinetics of the vacuum induction refining of silicon. Generally, the desorption of phosphorus atoms from the melt surface is assumed as the main mechanism for phosphorus evaporation from silicon. In all previous works

38

39

40

4142

43

44

45

46 47

48

49

50

5152

53

54

55 56

57

58

5960

61 62

6364

65

66

67

68

69

70 71

72

[3,4,43,65,69-73] the monoatomic and diatomic desorption of phosphorus at the melt surface have been assumed.

In our previous work $^{[6]}$ on vacuum refining of silicon at ultra – high temperatures (UHT, by definition $T_{UHT} \geq 1.25~T_{m,~Si}$) we showed the apparent mass transfer of phosphorus increases significantly when temperature of the refining approaches to UHTs $^{[6]}$. In the same work $^{[6]}$ we proposed the hypothesis of decomposition of transient silicon phosphides on melt surface to explain the acceleration of mass transfer of phosphorus to the gas phase. In this research, we applied KEMS to characterize the vacuum evaporation of phosphorus from liquid Si and will compare the obtained results with the results from the Si refining experiments. The results of this paper will provide an insight knowledge about Si – P system and hence will contribute to the field of Si refining.

Table 1. The recent studies on the thermodynamics of P and dilute solutions of P in liquid Si.

Study	Subject of research	Contribution to the field
Schlesinger [74]	The thermodynamic data of phosphorus and phosphorus gases (P, P ₂ , P ₄)	Gibbs free energy functions for evaporation of phosphorus species and formation of silicon phosphides
Zaitsev et al. [66]	Thermodynamics of dilute solutions of P in liquid Si by KEMS method.	Activity of P in dilute solutions of Si melt, Gibbs free energy of P ₂ gas evaporation from Si melt, detected mainly P ₂ ⁺ and reported P ⁺ by mass spectrometer.
Miki et al. [65]	Thermodynamics of dilute solutions of P in liquid Si by equilibration method.	Activity of P in dilute solutions of Si melt, Gibbs free energy of P ₂ gas evaporation from Si melt.
The phase diagram of $Si - P$ system in Si rich side by DSC/DTA method.		The liquidus and solidus for low P concentrations was studied.
Liang & Fetzer [64]	Modeling of Gibbs free energy of Phosphorus gases and phosphides in Si – P system.	Gibbs free energy of P, P ₂ , P ₄ and phosphides SiP, and SiP ₂

2 Experimental procedure

2.1 Si – P sample preparation

For this study, a Si – P alloy with 3715 \pm 200 ppmw of phosphorus was initially made by adding red phosphorus into 400 g of Si melt at 1500 °C. The alloying process was carried out in a graphite crucible (properties mentioned in ^[7]). For this purpose, polysilicon (FBR® purity 8N) was charged into the graphite crucible. Then it was melted in a vacuum induction furnace under Ar (6N) atmosphere, subsequently red phosphorus was added to the silicon melt and the alloy was then cast in a water-cooled copper mold. This Si – P alloy was then characterized by ICP – MS. More details about the silicon high phosphorus alloy production can be found in ^[42]. In order to study the gas phase over various melt phosphorus concentrations, we mixed and re-melted this Si high phosphorus alloy with proper amount of FBR® silicon (purity 8N) to provide three samples with phosphorus concentrations of about 3000, 1250, and 100 ppmw. These samples will be named Si – 3000 P, Si – 1250 P, and Si – 100 P, respectively in this paper. After the re-melting process the phosphorus concentration of each sample was measured by ICP – MS technique as 3100 ppma (\pm 136), 1227 (\pm 25), and 97.3 (\pm 2) respectively.

2.2 Knudsen effusion mass spectrometry (KEMS) study

Knudsen Effusion Mass Spectrometry (KEMS) was applied to study the gaseous species evaporating from the Si – P samples. The schematic representation of the KEMS machine applied in this research together with the setup configuration are shown in Figure 1. More details about this technique can be found in [59,76]. Here, as shown in Figure 1, the sample is heated up to the target temperature in a small enclosure with an orifice on top, called the Knudsen cell, which is assumed to provide the molecule – wall collisions dominating over molecule – molecule collisions in the gas phase [52]. The Knudsen cell is heated up in high vacuum conditions and the pressure condition in the Knudsen cell is low (lower than 10 Pa), leading to a molecular beam effusing out of the cell's orifice. Under these conditions the gases inside of the Knudsen cell can be considered as an ideal gas. If thermodynamic equilibrium in the cell is achieved, this means, that equilibrium is also achieved between the gas and the condensed phases. Therefore, from a thermodynamic point of view there is no difference, if species are formed in the gas phase or on the melt surface, their concertation will be determined by the equilibrium constant. The molecular beam is redirected to an ionization chamber, where the gas molecules get ionized in a strong electric field. The ions leaving the ionization chamber pass through an electromagnetic field, where they are classified based on their mass over charge (m/z) ratio.

Previous studies [7] indicated that the best refractory for holding liquid Si at high temperatures and vacuum conditions is graphite, while at the crucible/melt interface a SiC layer is spontaneously formed

and maintained. To minimize Si loss via SiC formation, our Si – P samples (about 50 – 75 mg) were put in a tiny SiC crucible with a height of 10 mm and an inner diameter of 7 mm. This crucible was put in a graphite Knudsen cell with an orifice of 0.3 mm diameter on the top. The Knudsen cell was then put in a tantalum crucible with a cap on it with 1 mm orifice in the center. Temperature of the cell was measured with pyrometer. In this case the measured temperature and actual temperature of the sample can deviate. Therefore, temperature and pressure calibration was performed with pure silicon (8N purity), which is also suitable for studied samples according to the applied temperature range. The melting point of Si was observed *in situ* with ion current signal by heating the sample with 1 °C/min. The measured ion current at the melting point was used to determine the calibration constant according to the equation:

140 _____

130

131132

133

134

135

136

137

138139

141

142143

144

145146

147

148149

150

151

152153

154155

156

157

158

159

160

161162

163

$$p_{t} = \frac{kI_{t}T}{\sigma_{t}} \tag{1}$$

where ksi is the sensitivity constant of the instrument, where ion currents of Si⁺, Si²⁺, Si³⁺ were considered with the assumption, that there is no further contribution from Si₂, Si₃ and Si₄ molecules, T is the temperature in K, and σ_{mol} is the ionization cross section of atoms or molecules. The cross sections of the atoms (σ_{at}) were taken from [77] at an electron ionization energy of 70 eV. In the case of molecules the total cross sections were calculated according to the equation: σ_{mol} = $0.75 \sum_{i} \sigma_{at}(i)$ [78]. Additional temperature calibration was also performed by using melting points of Ni and Ag (further details are available in [55,79]). Before running the experiment, the chamber of the KEMS machine was vacuumed down to 10⁻⁶ Pa and then the power was switched on. An average heating rate of 20 °C/minute up to 400 °C was applied, and then the temperature was increased up to 1100 – 1200 °C with a fast-heating rate (around 100 °C/min) through electron bombarding onto the tantalum crucible (this is not shown in Figure 1 for simplicity). At this point the Knudsen cell orifice was well aligned with the aperture. The sample was then heated up to about 1375 °C by 10 °C /min and it was held at this temperature for a while to attain a homogenous temperature distribution all over the cell. We did several preliminary experiments to characterize the possible gaseous species effusing out of the Knudsen cell and to check the fragmentation of the species in the ionization chamber. For this purpose, three different excitation voltages (15, 50, and 70 eV) with the emission current of 0.15 mA were applied to check the fragmentation of the species effusing out of the cell. Based on these results a constant excitation voltage of 70 eV was used in all further experiments. Subsequently, several spectra were recorded over the range of 10 to 200 m/z, where m/z indicates the mass over charge ratio for the ionized species. These spectra were recorded at various temperatures up to 1800 °C. Based on the preliminary results, we carried out isothermal and polythermal experiments, during which the intensity of the ionized species (ions) were measured over time. The effect of temperature on the phosphorus species evaporating from the silicon was also studied. For

this purpose, various samples were heated up to the target temperature. In the polythermal experiments, the sample was heated up step by step, with 25 °C increase for each step. Then the sample was held at each step for 1 hour and the intensities of the ionized species were characterized.

 After the KEMS experiments the remained Si in the crucible was digested in a solution of HNO₃ and HF. Then the liquid was characterized by ICP – MS to track the phosphorus content of the samples. Figure 2 represents the graphite Knudsen cell enclosure and the SiC crucible after an isothermal experiment at 1442 °C for 8 hours. The whole crucible was submerged in acid for digestion of the Si as shown in Figure 2d. The sample was kept in the acid solution for 24 hours at room temperature. Then all the Si in the crucible was dissolved in the acid. Figure 2e shows the same SiC crucible after digestion indicating all the Si was dissolved out. The weight of the SiC crucible after acid digestion was compared with its initial weight before KEMS experiment (measurements carried out with Mettler Toledo®, model Excellence, 0.1 mg readability). There was not any sensible weight change. After the digestion the liquor was then characterized by ICP – MS (ICP – MS, Agilent – 8800 ICP-MS Triple Quad).

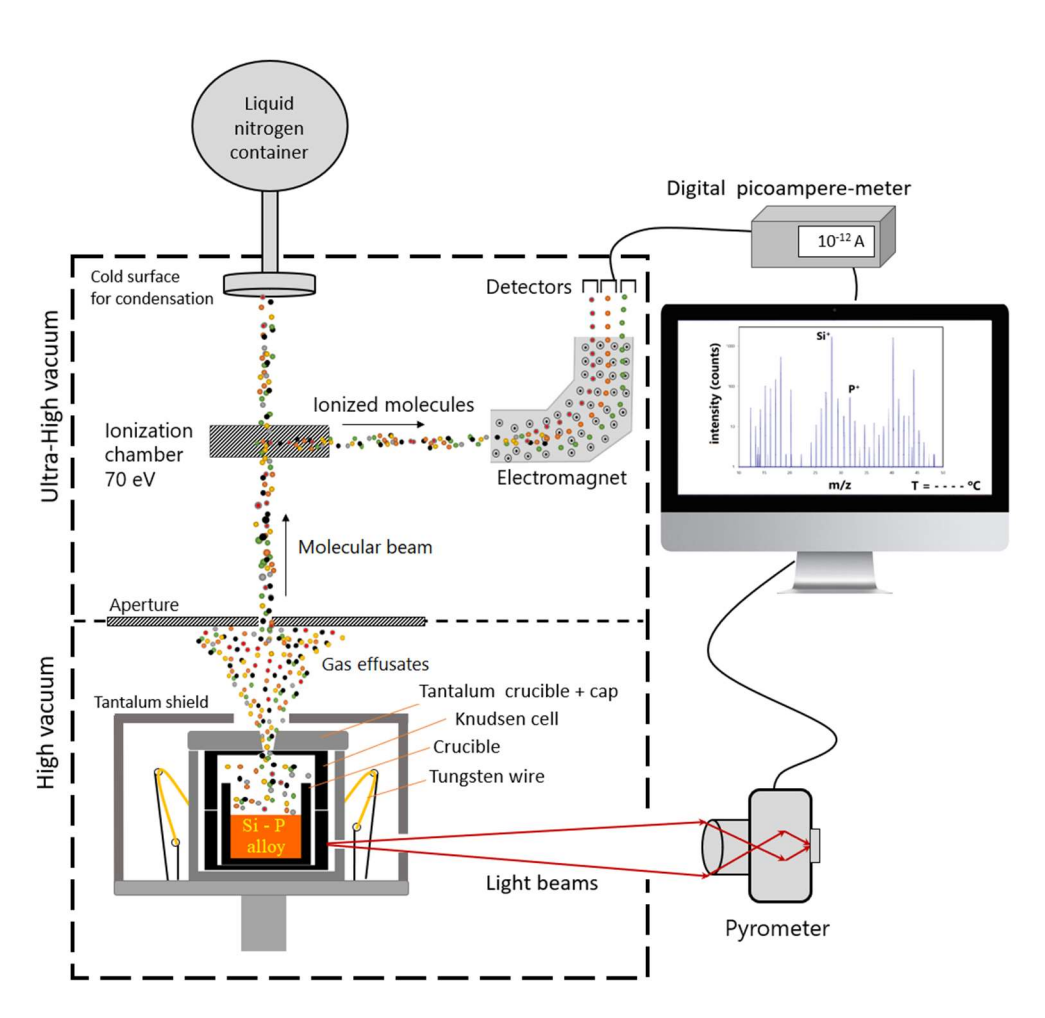
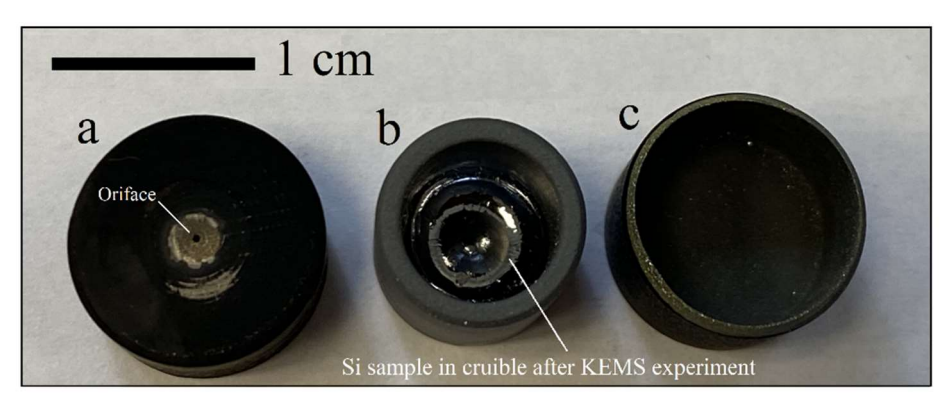


Figure 1. The schematic representation of the KEMS machine applied in this study.



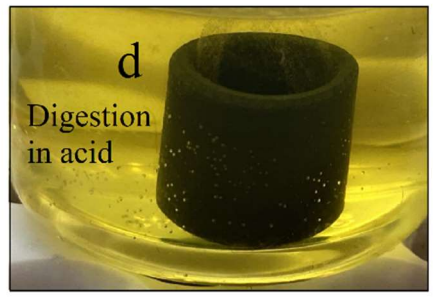




Figure 2. The top part (lid with orifice) of the graphite Knudsen cell (a), SiC crucible sample holder and Si sample after 8 hours in 1442 °C (b), the Knudsen cell without its lid (c), the SiC crucible submerged in acid when Si sample is digested (d), SiC crucible after complete Si digestion (e).

3 Results

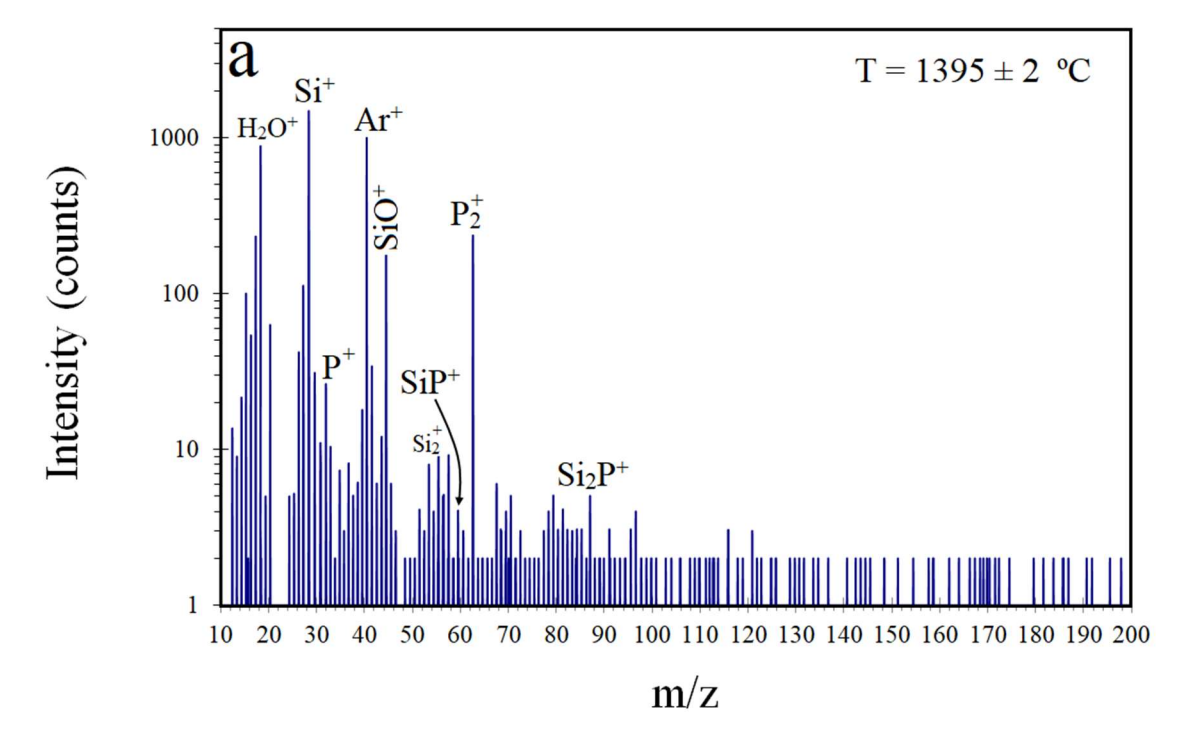
The obtained KEMS results from the isothermal and non-isothermal experiments are presented and discussed in this section. The preliminary experiments were carried out in isothermal condition to characterize the gaseous species and the results are presented in section (3.1), and the effect of temperature is studied by polythermal experiments, presented in section (3.2).

3.1 Isothermal KEMS experiments

3.1.1 Evaporation below and above the liquidus

Figure 3 presents two obtained mass spectra by evaporation of the Si - 1250 P sample taken of the solid sample and immediately after melting of the silicon via rapid heating to 1500 \pm 2 °C. It is worth mentioning that it took about 20 minutes to record each mass spectrum shown in Figure 3. The temperature was fixed while recording the spectra. The spectrum taken from the solid silicon at 1395 °C (Figure 3a) indicates that Si⁺ (m/z 28) is the dominant species. In addition, some phosphorus species can be detected in gas phase as P_2^+ (m/z 62) and P_2^+ (m/z 31) with high intensities, and SiP⁺ (m/z 59) and Si₂P⁺ (m/z 87) ions with low intensities. Figure 3b shows the intensities of P_2^+ and P_2^+ species become stronger when the sample is melted. In addition, it can be seen that P_2^+ is the dominant gaseous

species and the intensities of P₂⁺ is five times of that for Si⁺ (m/z 28). It also shows other phosphorus 206 species like P_4^+ (m/z 124), SiP_2^+ (m/z 90) and Si_3P^+ (115) with considerable intensities and P_3^+ (m/z 207 208 93) barely detectable. Obviously, we could detect phosphorus in the form of SiP+, Si₂P+, Si₃P+, and SiP₂⁺ as new results, in addition to the reported P₂⁺ and P⁺ species in literature over dilute solutions 209 of phosphorus in silicon. The ion intensities of the phosphorus species detected by mass spectrometry 210 211 in Figure 3 are presented in the supplementary data. It should be mentioned that the detected Ar⁺(m/z 212 40) and H₂O⁺(m/z 18) ions are coming from the remained gas in the chamber and the SiO⁺(m/z 44) is 213 from the reaction of remained oxygen and Si. 214 The only previous mass spectrometry study of the Si – P system was carried out by Zaitsev et al. in ^[66] where they studied Si – P samples with various concentrations of phosphorus over $x_{\underline{P}} = 0.0035$ – 215 0.265. However, they reported only the P⁺ and P₂⁺ species. In addition, they mentioned the intensity 216 of P^+ was only 2% of that of P_2^+ , and concluded that the P^+ is the result of P_2^+ fragmentation in the 217 ionization chamber ($P_2 + e^- = P^+ + P + 2 e^-$, $\Delta E = 15.56 \text{ eV}$). However, as mentioned in the 218 219 experimental procedure the studies on the ion fragmentation were carried out by trying various ionization voltages ($\Delta E = 15, 50, 70 \text{ eV}$), during which P⁺ ion peak was detected with the same 220 intensity in all the cases. This indicates that the P⁺ ion is coming from the ionization of the P atoms 221 $(P + e^- = P^+ + 2e^-, \Delta E = 10.49 \text{ eV})$ and hence P^+ ions represent the monoatomic phosphorus in 222 the molecular beam, effusing out of the Knudsen cell. In addition, we studied the fragmentation of 223 224 various Si ions (Si⁺, Si₂⁺, Si₃⁺, Si₄⁺) at various temperatures and concluded that the Si⁺ ion is coming mainly from ionization of monoatomic Si gas species. The fragmentation of the Si ions is studied by 225 Tomooka et al. [80] and they have shown the Si⁺ ion, comes from the monoatomic Si gaseous species. 226 227 The discussion about fragmentations is beyond the scope of this paper and further information can be found in [80]. 228



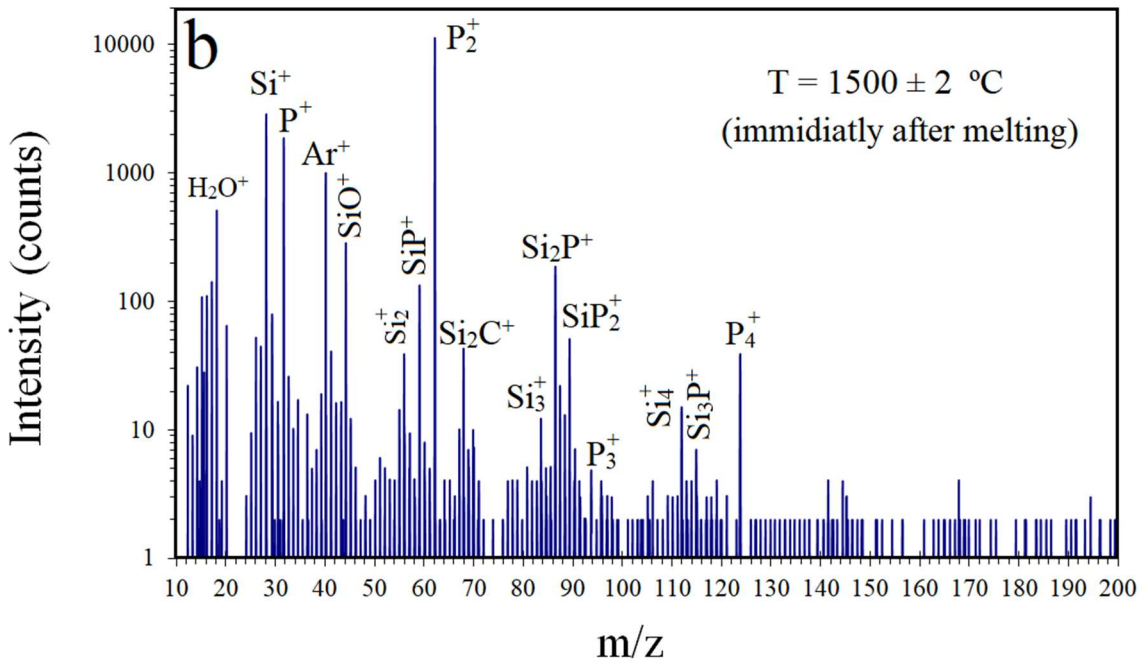


Figure 3. The KEMS raw spectra of a Si-1250 P sample; before sample melting (a), and immediately after the melting and heated up to 1500 °C (b).

3.1.2 Effect of melt composition changes

239

240

241

242243

244

245

246

247

248

249

250

251

252

253

254

255256

257258

259

260

261

262

263

264265

266267

268269

270

271

272273

In order to study the phosphorus species evaporating from Si with time, we did a long-term isothermal experiment at 1442 ± 2 °C on the Si – 1250 P sample as shown in Figure 4. The intensities of various species were measured in one-hour intervals. It should be mentioned that it took about 1 hour from the melting point of Si to make the temperature steady on 1442 °C. Then the characterization was started, and hence, the changes taking place over this time were not recorded. The results are presented in Figure 4(a) indicating the ion intensity of all phosphorus species decreased over the time. This is due to the decrease of the phosphorus concentration in the Si melt. In the first measurement, the P₂⁺ and P⁺ are the most dominant phosphorus species with close intensities in the gas phase. However, we see that P₂⁺ loses its intensity faster than P⁺, and P⁺ is the most dominant form of phosphorus species effusing out of the Knudsen cell at longer times. The intensities of Si₂P⁺ and SiP⁺ at the first measurement are significantly lower than P₂⁺ and P⁺, and higher than that of P₄⁺. Like all the phosphorus compounds, the intensities of Si₂P⁺ and SiP⁺ decreased over time, and as it is obvious in Figure 4. Low intensities of P₄⁺ were detected in the experiment in comparison with the above species, while SiP_2^+ was not detected in this sample, probably due to lower P^+ concentration compared with the preliminary test at 1500 °C. Considering the data in Figure 4, it is obvious that the intensity of Si⁺ was constant during the time of the experiment, while the intensities of all phosphorus species decreased over the experiment time. This may indicate that the equilibrium condition (at least in short time intervals) was established for Si in the Knudsen cell and the saturated vapor pressure was achieved, but not for the phosphorus species. In this case, the reduction of vapor pressure is due to evaporation of phosphorus from the solution. Having the ion intensities of various compounds, we can calculate the vapor pressure of each species by applying the well – known KEMS equation presented as follows:

$$p_i = \frac{kI_iT}{\sigma_i} \tag{2}$$

Where the p_i denotes the vapor pressure and the I_i is the intensity of the ion species i, T is absolute temperature in Kelvin, σ_i (cm²) is ionization cross section at 70 eV, and k is the sensitivity constant of the instrument. In order to determine the ion cross sections of the molecules, the total cross sections were calculated by the equation $\sigma_{molecule} = 0.75 \sum_i \sigma_{atom}(i)^{[59]}$. All the used cross sections of the species are reported in Table 2. To determine the instrument sensitivity coefficient (k), we inserted the ion intensity of Si⁺ (I_{Si} ⁺) into equation (1) while the pressure of Si⁺ (p_{Si} ⁺) was taken from p_{Si} ⁻ to obtain p_{Si} ⁻ (Pa cm² counts-1 K-1) at 1442 °C.

Having all the required terms of equation (1), the vapor pressures of the ions at 1442 °C are calculated and depicted in Figure 4(b). This figure indicates that the vapor pressure of all phosphorus compounds

reduces by experiment time since the x_P is reduced. After 8 hours of keeping the sample at 1442 °C, the sample was immediately cooled down to below the Si melting point in some seconds to prevent the composition change of the liquid Si. Therefore, the phosphorus concentration in the Si left in the crucible will represent the x_P in liquid Si for the last study point shown on Figure 4b. This sample after the experiment was characterized by ICP – MS (as mentioned in the experimental procedure and Figure 2). The concentration of phosphorus in liquid silicon (in molar fraction, x_P) of the last point of the experiment was determined as $x_P = 20.03$ ppma, as shown in Figure 4(b).

Table 2. Ionization cross section of various species at 70 eV.

Species	σ ,10 ⁻¹⁶ (cm ²)
Si	4.905
P	4.2564
P_2	6.3846
P_3	9.5769
P_4	12.7692
SiP	6.87105
Si_2P	10.5498
Si_3P	14.22855
SiP_2	10.06335

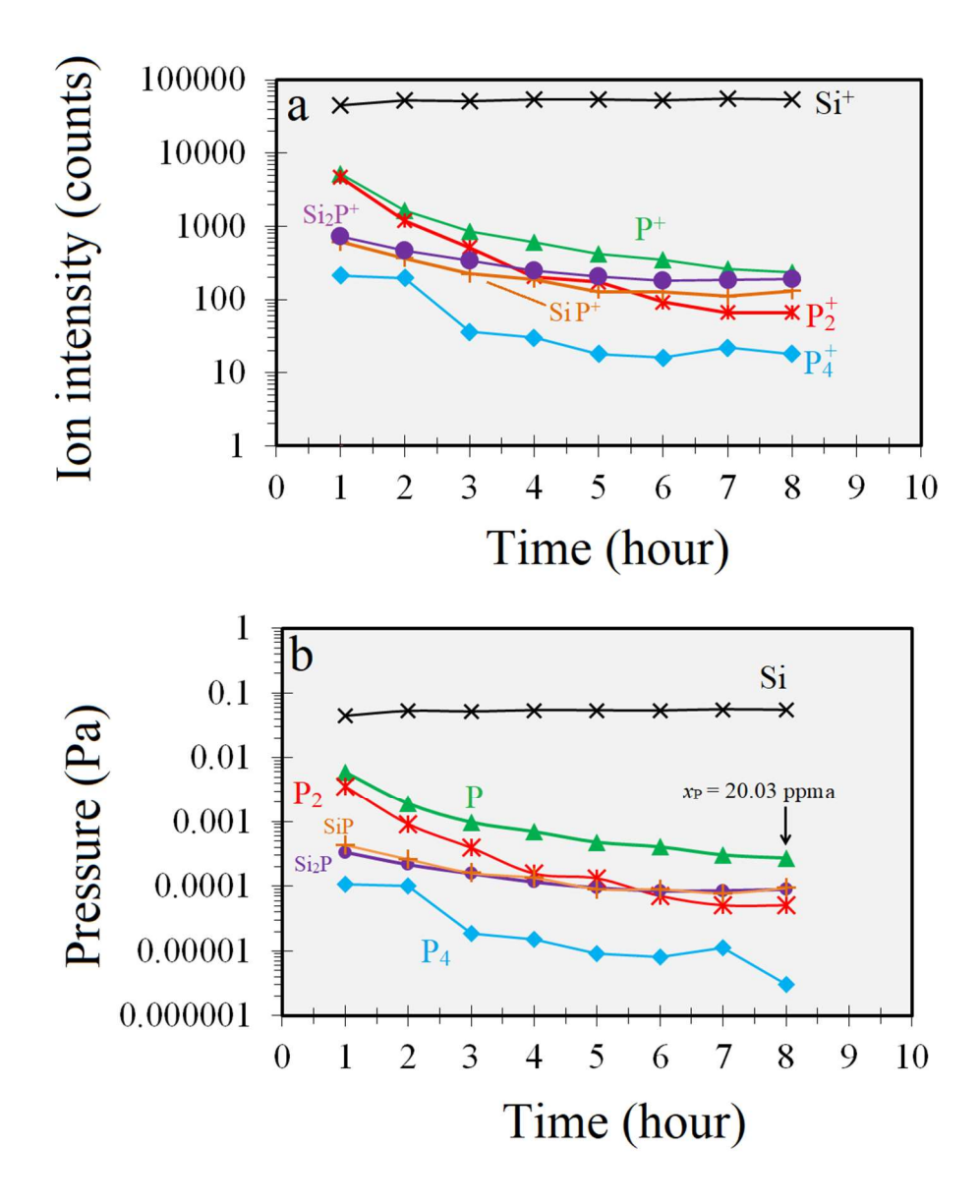


Figure 4. The ions intensities in the isothermal experiment of Si - 1250 P sample at 1440 ± 2 °C (a), and their corresponding calculated pressures (b).

3.2 Polythermal KEMS experiments

3.2.1 Temperature effect

Figure 5 shows the ion intensities of the phosphorus species evaporated at various temperatures for the Si – 3000 P sample. In this sample, we had intensive evaporation due to the high content of P in Si, which could damage the instruments. Therefore, we only measured five species (Si, P, P₂, P₄, and SiP). Figure 5 shows that Si exhibits a symmetrical profile over the heating and cooling cycles which indicates the steady state was established for Si evaporation in the Knudsen cell. However, it is not the case for phosphorus containing molecules. It is obvious from Figure 5 that the intensities of all phosphorus containing species are reduced both in the heating and cooling cycles, which happens due

to the depletion of P in melt. The purpose of presenting Figure 4 was to indicate the phosphorus content is always decreasing in the Si-P sample due to faster evaporation and loss compared to Si and hence it leads to the reduction of the intensities of the phosphorus containing species. However, we will show that temperature has a bigger effect and at higher temperatures the intensities of phosphorus containing species increase again.

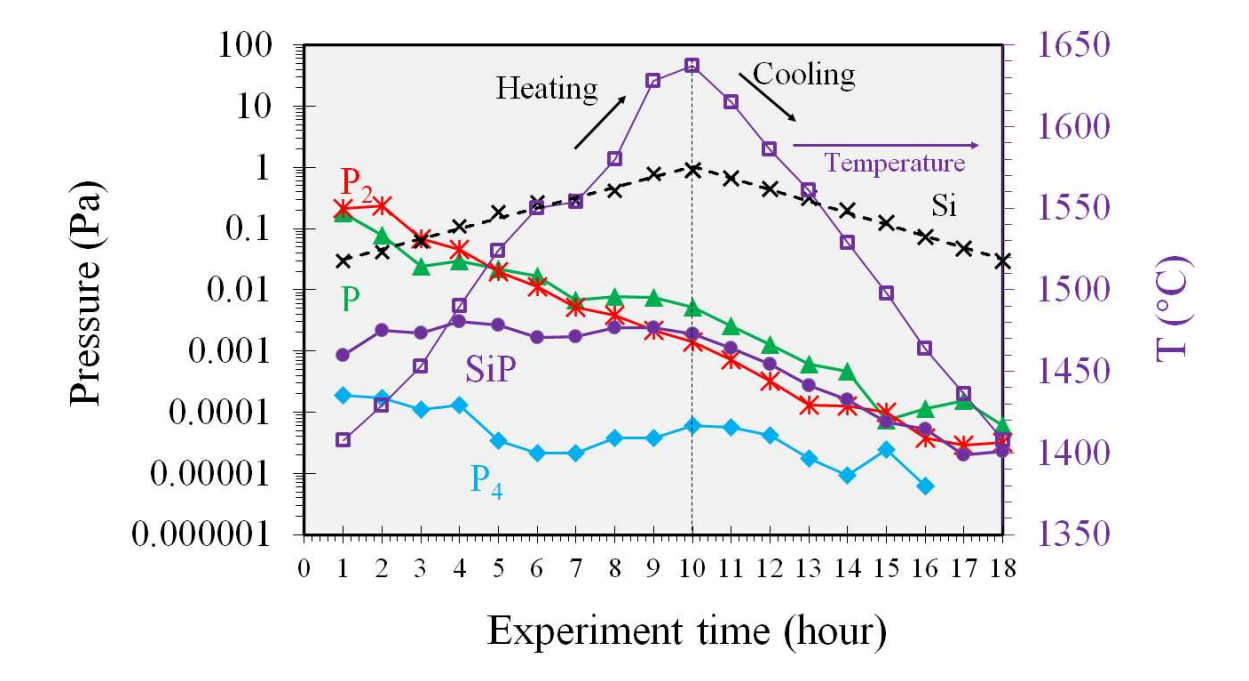


Figure 5. Effect of temperature on the vapor pressure of various compounds in Si - 3000 P sample over heating and cooling cycle.

3.2.2 Phosphorus concentration and temperature changes

In order to get a better view of the temperature effect on the evaporation of phosphorus species from Si melt, we characterized three samples with various phosphorus contents in liquid Si. The vapor pressures of the studied species in the polythermal experiments are calculated by applying equation (1) and the results are shown in the Figure 6. The raw data from KEMS experiments, including the ion intensities can be found in the supplementary data of this paper. Figure 6 shows that the vapor pressure of Si has an exponential relation with temperature for all samples, which is reliable. The vapor pressure of silicon from literature [81], which is also plotted in Figure 6, is in good agreement with our measurements. However, the vapor pressure of phosphorus species decreases by the temperature increase in both the heating and cooling cycles, because of the phosphorus concentration decline in the liquid Si. Figure 6 indicates that the pressure of P₂ is dominant at the beginning for all the samples

(regardless of the initial x_P), and it is declining faster compared to the other species, which agrees with the isothermal experiment (Figure 4). In addition, Figure 6 indicates that the interception point of P_2 with P shifts toward higher temperatures when initial phosphorus content in the samples is higher, as the interception temperatures are 1450, 1470, and 1550 °C in the samples Si – 100 P, Si – 1250 P, and Si – 3000 P, respectively. The change in P_4 intensity with increase in temperature is interesting. P_4 intensity initially decreases and then it increases upon heating to 1550 – 1600 °C, following with a subsequent intensity rise at higher temperatures. However, in the Si – 3000 P sample the pressure of P_4 is higher at the beginning and decreases by increasing the temperature, but then it increases when temperature exceeds 1550 °C.

The obtained data in Figure 6 reveals that, for the sample Si – 100 P, the phosphorus evaporation for this sample takes place intensively by means of SiP, Si₂P, and Si₃P especially when temperature exceeds 1680 °C. Figure 6 shows that the evaporation of silicon phosphides comprises an important part of phosphorus evaporation from the Si – 1250 P sample. However, P was always the dominant species, getting higher intensities with simultaneous P₂ intensity decline. Comparing samples Si – 100 P and Si – 1250 P, it could be concluded that silicon phosphides are the dominant forms in the vapor when the phosphorus content in the sample is low and the temperature is higher, above 1650 °C. It should be mentioned that since the intensive evaporation of phosphorus species are detrimental for the instrument, therefore, we had to limit the number of the species to be characterized limit temperature range in the samples with higher amounts of phosphorus. For this reason, in the sample Si – 3000 P, only SiP was recorded as a representative of the other silicon phosphides in this sample. Regarding the results presented by the isothermal experiments and this section, we can summarize the various phosphorus containing species evaporating from Si and their condition as it is presented in Table 3.

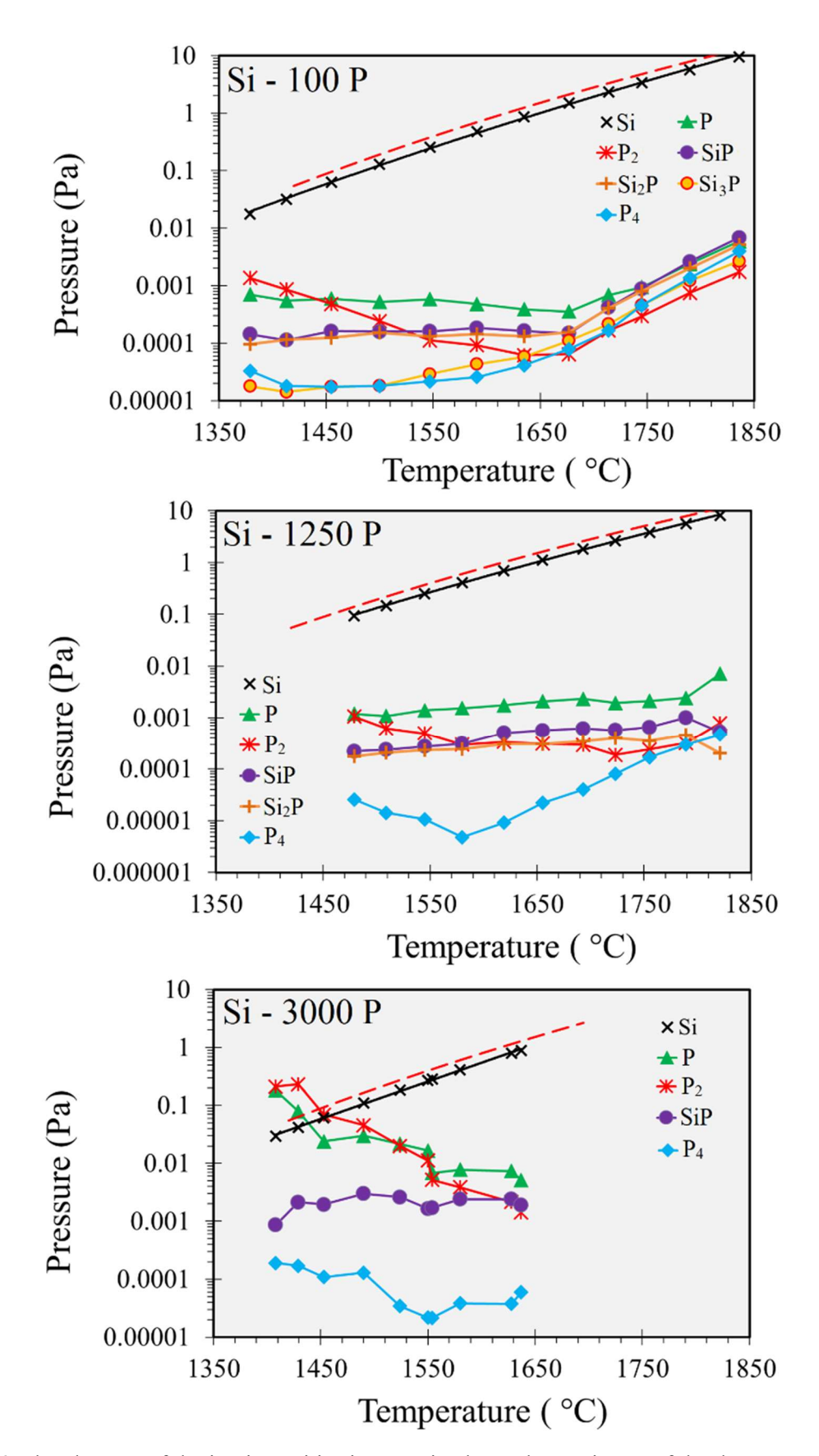


Figure 6. The changes of the ion intensities in non - isothermal experiment of the three samples. The vapor pressure of Si from [81] is inserted for comparison (red dashed line).

Table 3. The detection conditions of various phosphorus containing ions in mass spectra during of isothermal and polythermal experiments.

Ions	Detection condition and interpretation	
	The dominant phosphorus species when Si is solid and at the beginning of melting. Dealines in the line of the melting.	
	Declines immediately after melting. On 1650.00	
P ₂ +	Slightly increases at high temperatures than 1650 °C.	
_	Depends highly on P content in Si.	
	Detected when Si was solid as well.	
	Second highest intensities at the beginning of experiments and it declines by time.	
	Becomes the dominant species when	
P ⁺	P ₂ ⁺ is declined over 1450 °C – 1550 °C depending on P content in Si.	
	It increases by temperature.	
	Is stable in all temperatures and is the main phosphorus species when P content decreases.	
	Detected only in liquid Si.	
	Detected at the beginning of experiments (more for higher P contents)	
P ₄ +	• Increases intensively beyond 1550 °C – 1600 °C and higher temperatures.	
-4	• Depends on x_P in liquid Si and evaporates intensively beyond 1550 °C – 1650 °C.	
P.+	Was detected barely only at the beginning of experiment after melting of Si and in high	
P ₃ +	phosphorus-containing samples.	
	Not a dominant phosphorus species in Si – P system.	
	Slightly detected at low temperature even when P content was high.	
g. 54	• Increases intensively with temperature even when P content is low.	
Si ₃ P ⁺	Depends on temperature and intensifies by silicon evaporation at higher temperatures.	
	Detected in all samples with the same intensity at low temperatures.	
	Increased with temperature.	
Si ₂ P ⁺	Depends on temperature and is less dependent on P content.	
	Detected in all samples with the same intensity at low temperatures.	
	Increased with temperature.	
SiP ⁺	Depends on temperature and is less dependent on P content.	
SiP ₂ ⁺	 Depends highly on P content in Si and is observed at temperatures close to liquidus. Only detected in Si – 3000 P sample and disappeared rapidly after some phosphorus loss. 	

4 Discussions

In this section we apply the results from the isothermal experiment to discuss the dependency of the vapor pressure of the phosphorus species to the x_P in Si at 1442 ± 2 °C. In addition, the results from polythermal experiments will be applied to discuss the mechanisms of phosphorus evaporation from silicon and will be compared with the obtained data from vacuum refining studies ^[6]. We will discuss the liquid-vapor equilibrium of Si – P system in section (4.1) and then the various forms of phosphorus mass transfer from melt surface to gas phase (evaporation) in section (4.2). At the end we present the possible mechanisms of phosphorus evaporation at the melt surface in section (4.3).

4.1 Liquid-vapor equilibrium for Si – P system

The thermodynamic properties of vapor components in the Si - P system at elevated temperatures are summarized in Table 4. We can apply the following relations to calculate the vapor pressure of various phosphorus species in equilibrium with liquid Si, using the following relations:

$$p_{\rm P} = p^{\circ} x_{\underline{P}} \gamma_{\underline{P}}^{\infty} exp\left(-\frac{\Delta G^{\circ}_{ii+} \Delta G^{\circ}_{iii}}{RT}\right)$$
 (3)

$$p_{P_2} = p^{\circ} \left(x_{\underline{P}} \gamma_{\underline{P}}^{\infty} exp \left(\frac{-\Delta G^{\circ}_{iii}}{R T} \right) \right)^2$$
 (4)

$$p_{\mathrm{P}_{4}} = p^{\circ} \left(x_{\underline{\mathrm{P}}} \gamma_{\underline{\mathrm{P}}}^{\circ} exp \left(-\frac{\Delta G^{\circ}_{iii} - 0.25 \Delta G^{\circ}_{i}}{\mathrm{R} \, T} \right) \right)^{4} \tag{5}$$

Where $x_{\underline{P}}$ and $\gamma_{\underline{P}}^{\infty}$ are the phosphorus molar fraction in liquid Si and the activity coefficient of phosphorus in melt, respectively, R is the universal gas constant (8.314 J·mol⁻¹·K⁻¹), and T is absolute temperature in Kelvin. The parameter p° is the reference pressure of the gaseous phosphorus. When applying the relation introduced by Zaitsev et al. ^[66], we need to put the saturated vapor pressure of phosphorus at the studying temperature ^[74]. However, when dealing with the model introduced by Miki et al. ^[65] we need to assume $p^{\circ} = 101325$ Pa. In addition, whenever the model of Miki et al. is applied, phosphorus weight per cent in liquid silicon (P wt.%) should be considered as the concentration and the weight per cent interaction coefficient (f_P) should be assumed to be unity. Zaitsev et al. ^[66] criticized the relationship introduced Miki et al. ^[65] for being misprocessed and showed that a right processing of the data that was produced by Miki et al., will be in good agreement with the Zaitsev et al. measurements for P₂. Therefore, we will apply Zaitsev et al.'s relation in this paper.

Figure 7 shows the equilibrium vapor pressure of phosphorus containing species at 1442 ± 2 °C

Figure 7 shows the equilibrium vapor pressure of phosphorus containing species at 1442 ± 2 °C calculated according to equations from (2) to (4) and with FactSage® (version 7.3 and SGTE database). The experimental data from this research obtained by KEMS are also shown in Figure 7. Obviously,

our measured vapor pressure of P2 is in good agreement with the Zaitsev et. al measurements [66] and calculations from FactSage®. However, it is not the case for other species (P, P₄, Si₂P, SiP). Figure 7 indicates that FactSage® calculations underestimate the vapor pressure of P, SiP, and Si₂P about 10 times of this research measurements. However, in the case of P₄, both FactSage[®] and equation (4) underestimate the vapor pressure about 10 billion times. Figure 7 indicates that equation (2) and (4) overestimate the vapor pressure of P about 10 times. This could be due to the inaccuracy of the Gibbs energy for the reactions (i) and (ii) and hence the equations (2) and (4) cannot predict the correct vapor pressure of P and P₂. In addition, we calculated and inserted the vapor pressure of P₃ by applying the intensity of the P₃⁺ ion detected in the spectrum of the sample Si – 1250 P at 1500 °C, presented in Figure 3b. Figure 7 shows the vapor pressure of P₃ calculated from FactSage® is at least 100 times lower than our measurements. We should mention that the experimental data presented in this research is unique over the concentration range and are not reported elsewhere. Therefore, the differences between the obtained experimental data with the SGTE database [82] could be due to extrapolation of data or modelling, which can explain the deviations observed in Figure 7. Hence, the experimental results of this research can contribute to increasing the accuracy of the thermodynamic data for the Si – P system.

400401

402403

404

405

406

407

408

409410

411

412413

414

415

416417

418

419420

421

422

423424

425

426427

428

429

430

431

432

As mentioned before Zaitsev et al. [66] only reported P2 ions in the Si - P system and not any other phosphorus ions. However, we managed to measure the vapor pressure of the P, SiP, Si₂P, and P₄ in addition to P₂. From Figure 7 it is obvious that the vapor pressure of P₂ (for 20.03 ppma P in Si) measured in this research is exactly on the line already introduced by Zaitsev et al. [66]. If we had the corresponding x_P of each data point shown in Figure 4, we could plot the vapor pressure lines for each species over the over the phosphorus concentration in melt. Since we showed the vapor pressure of P₂ can be read by Zaitsev et al. [66] relation, the data for the vapor pressure of P₂ can be put on the P₂ line in Figure 7, one by one to obtain the corresponding x_P in liquid Si for each studied point. Having the $x_{\rm P}$ in hand, the vapor pressures of the phosphorus species already shown in Figure 4 are plotted versus the obtained x_P as presented in Figure 8. For this, The data points presented in solid fill in Figure 8 are plotted versus the measured x_P by ICP – MS and the rest of the data are plotted versus the x_P calculated by the aforementioned method. As can be seen, there is a good correlation among the data for each species and the obtained lines in Figure 8 have a high value of squared-R, indicating on the precision of the applied technique to calculate the x_P in the isothermal experiment. Figure 8 shows the dependency of the phosphorus species vapor pressures as function of x_P at T = 1442 °C, and the vapor pressure formula for each species as a function of x_P is also presented in the Table 5.

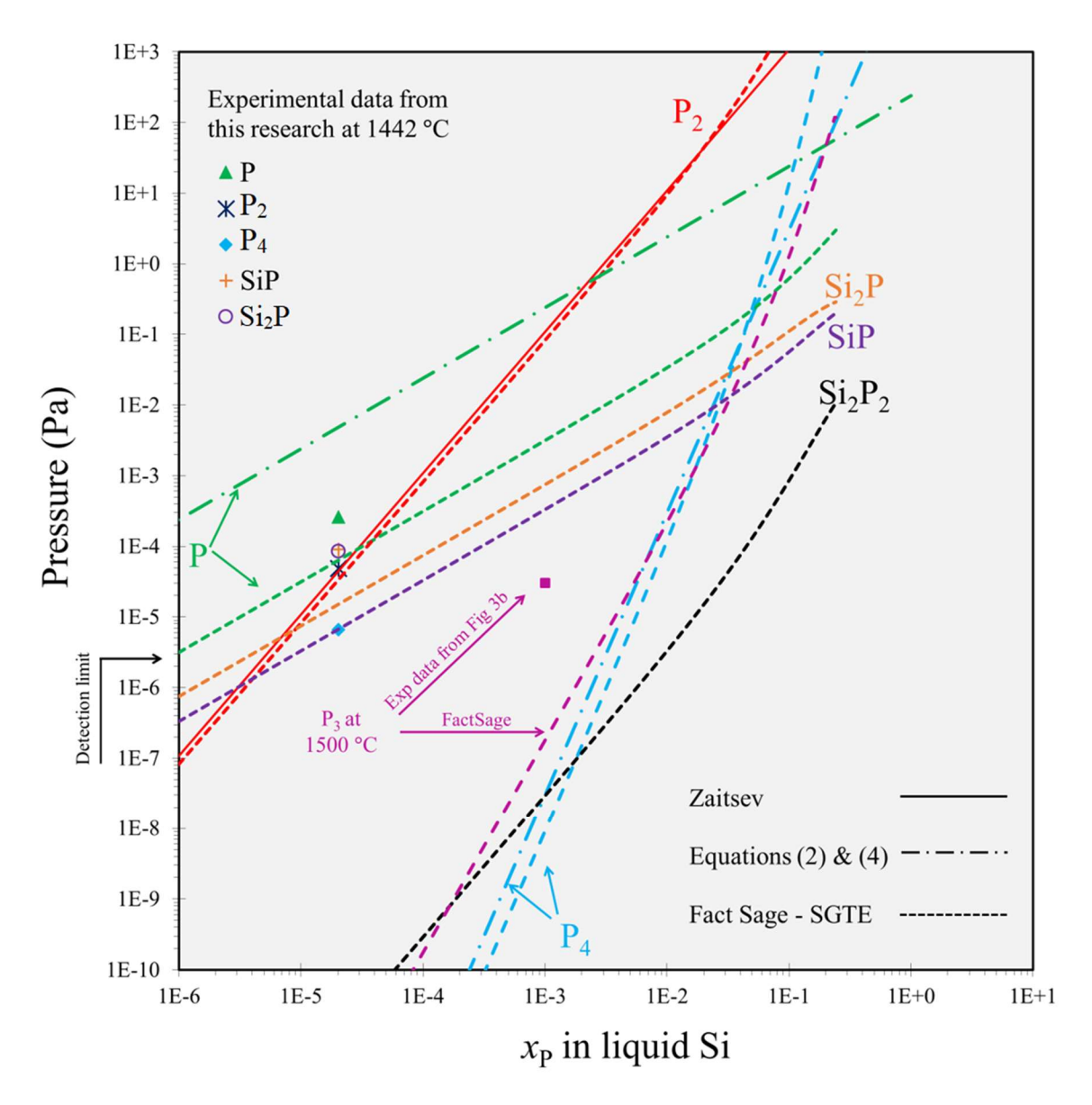


Figure 7. The equilibrium vapor pressure of P – containing species in equilibrium with liquid Si at 1442 °C. The curves are plotted from relations presented in literature: Zaitsev et al. [66], Schlesinger [74], and using FactSage – SGTE [83].

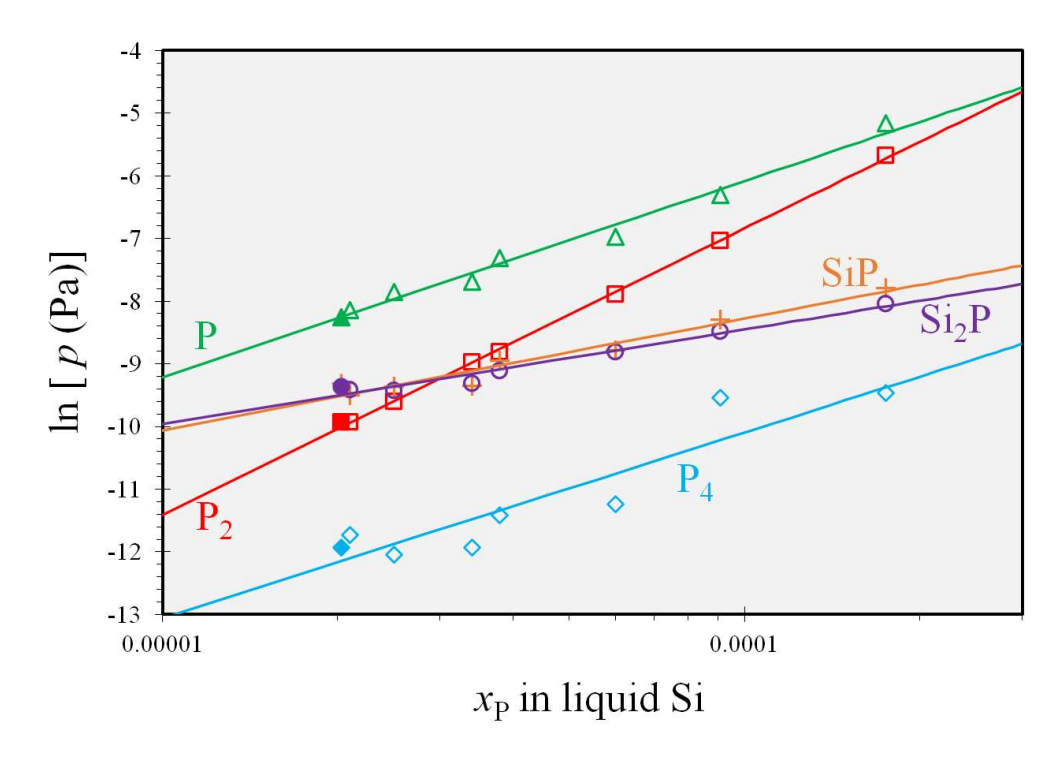


Figure 8. The measured equilibrium vapor pressures of phosphorus – containing species over dilute Si-P melts at 1442 ± 2 °C.

Table 4. Various phosphorus dissolution reactions in silicon melt and their corresponding Gibbs energy relations.

Relation no.	Relations and Thermodynamic functions	References
(i)	$\begin{aligned} &P_{4(g)} = 2P_{2(g)} \\ \Delta G^{\circ} \left[J \cdot mol^{-1}\right] = & -229500 + 154.5 \text{ T} - 0.00313 \text{ T}^2 \end{aligned}$	Schlesinger [74]
(<i>ii</i>)	$0.5P_{2(g)} = P_{(g)}$	Schlesinger [74]
()	$\Delta G^{\circ} [J \cdot mol^{-1}] = 248000 - 59.4 T$	
(iii)	$\underline{P} = 0.5 P_{2(g)}$ $\Delta G^{\circ} [J \cdot mol^{-1}] = 99500 - 29.46T$	Zaitsev et al. [66] (Reference state for phosphorus is pure phosphorus)
(iv)	$\underline{P} = 0.5 P_{2(g)}$ $\Delta G^{\circ} [J \cdot mol^{-1}] = 139000 (\pm 2000) - 43.9 (\pm 10.1)T$	Miki et al. [65] (Reference state for phosphorus gas is 1 atm)
(v)	$\ln(\gamma_{\underline{P}}^{\infty}) = 2.08 - \frac{4766}{T}$	Calculated from Zaitsev et al. [66]
(vi)	$log(p_{Phosphorus}[Pa]) = 9.965 - 2740/T$	Schlesinger [74]

Table 5. The obtained vapor pressures for various phosphorus species at 1442 °C as a function of x_P in liquid Si

Gaseous compound	ln [p (Pa)] at 1442 °C	
Р	$1.362\ln(x_{\rm P}) + 6.4602$	
P ₂	$0.8686 \ln(x_{\rm P}) + 5.0356$	
P ₄	$1.2864 \ln(x_{\rm P}) + 1.7528$	
SiP	$0.7735 \ln(x_{\rm P}) - 1.1535$	
Si ₂ P	$0.6566 \ln(x_{\rm P})$ - 2.4033	

4.2 Mass transport of phosphorus via evaporation

It is obvious from equation (1) that $I_i \cdot T$ is proportional to its pressure at any temperature. Since the pressure of species i is proportional to the number of the moles of i ($p_i = n_i p_t/n_t$) in the vapor, the number of moles of the species i effusing out of the cell is proportional to I_i . Now, considering the various phosphorus species detected in the KEMS experiments, we can obtain a measure of the overall number of phosphorus atoms leaving the melt surface in the form of all the phosphorus containing species presented above through the following relation:

$$A_{t-P}$$
 [intensity / cm²] = $\sum \frac{\kappa I_i}{\sigma_i}$ (6)

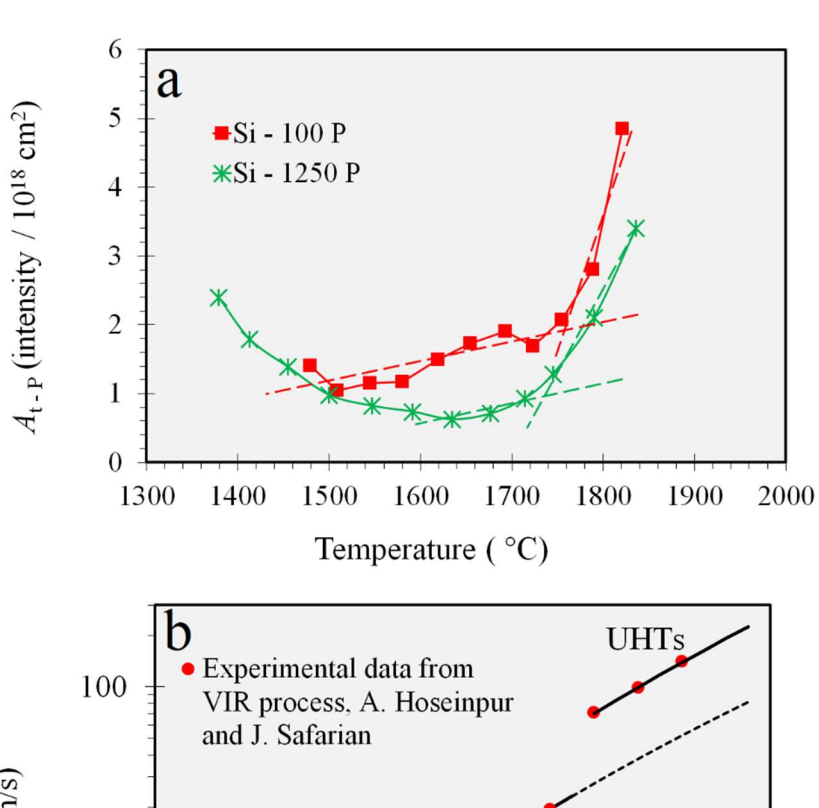
Where A_{t-P} is a measure proportional to the total numbers of the phosphorus atoms effusing out of the Knudsen cell (removed from silicon), I_i denotes the measured intensity of P – containing compound i (i = P, P₂, P₄, SiP, Si₂P, Si₃P, SiP₂), and κ is the number of the phosphorus atoms in the species i (e.g. κ = 4 for P₄). Equation (5) shows that the tetratomic and diatomic phosphorus molecules have greater impact on the total number of removed phosphorus atoms. This means that, even if the amounts of diatomic and tetratomic phosphorus molecules are less than the others, they may contain more phosphorus atoms and hence could have greater effect on the phosphorus evaporation (removal) rate. The changes of the calculated A_{t-P} with temperature for both the Si -100 P and Si – 1250 P samples are plotted in Figure 9a. Obviously, the total mass of phosphorus species evaporated decreased with increasing temperature from the melting point to 1650 °C due to the phosphorus loss from the system. However, A_{t-P} is showing rapid rise with increasing the cell temperature at above this temperature range. Plotting tangents over the obtained I_{t-P} curves, we see that A_{t-P} is significantly increased once the temperature exceeds 1730 and 1750 °C, for Si – 100 P and Si – 1250

samples, respectively. This increase in the mass transport of phosphorus in evaporation could be attributed to the intensive evaporation of silicon phosphides and P₄ as observed in Figure 6. Here it is worth to compare these results with our previous work [6] about vacuum induction refining of Si, for refining of 400 g of melt with below 15 ppmw of phosphorus in liquid Si, where we determined the mass transfer coefficient of phosphorus $(k_{\rm P})$ at 1500-1900 °C under isothermal conditions. The results from our previous work $^{[6]}$ showed that there is a large increase in the k_p at ultra – high temperatures (defined as T > 1762 °C = 1.25 $T_{\rm m,Si}$) via a change in the mechanism of chemical evaporation reaction. The previously obtained $k_{\rm P}$ for phosphorus removal from Si is plotted over temperature in the Figure 9b, indicating that the $k_{\rm P}$ is changed with temperature in a significantly higher rate when temperature exceeds about 1750 °C, in average 2.6 times higher than the prediction by extrapolating k_P from lower temperatures results. A comparison of Figure 9a with Figure 9b helps us to explain the significant k_P increase at 1750 °C. In our previous works [6,41] we used the first order kinetic model to explain the phosphorus concentration changes in the Si over time. When it comes to the application of vacuum evaporation of phosphorus for the refining of Si, it is important to have a knowledge about the share of various phosphorus species on the removal of phosphorus. As mentioned above some of the species contain more than one phosphorus atom, hence they may have greater impact on phosphorus removal from silicon. To formulate the contribution of each species in the overall phosphorus removal from silicon, we introduce the following relation:

 $\chi_{\mathbf{i}}[\%] = \frac{\kappa(I_i/\sigma_i)}{A_{\mathsf{t-P}}} 100 \tag{7}$

Where χ_i denotes the impact of species i ($i = P, P_2, P_4$, SiP, Si₂P, Si₃P) in the total phosphorus evaporation from silicon, which is called here "the evaporation impact". Figure 10 depicts χ_i for Si - 100 P and Si - 1250 P samples for non-isothermal trial. In this figure we have presented the sum of the phosphides (SiP, Si₂P, Si₃P) and hence we can simply compare the share of P removal in the form of silicon phosphides evaporation with the molecular evaporation. Figure 10 shows that at lower temperatures (T < 1500 °C) the monoatomic and diatomic phosphorus evaporation are the dominant mechanisms for phosphorus evaporation from silicon. In addition, it is obvious that by increasing the temperature the evaporation of silicon phosphides becomes considerable. Figure 10a indicates that for the Si - 100 P sample, the evaporation of silicon phosphides is the main mechanism of phosphorus removal for T > 1650 °C. Beyond 1720 °C the evaporation of P₄ becomes the second most effective form of phosphorus evaporation from silicon. It is obvious from Figure 10a that for the very dilute solution of P in Si (here below 100 ppm) at temperatures above 1750 °C almost 71 - 76 % of phosphorus removal is by means of P₄ and silicon phosphides evaporation. However, Figure 10b indicates that the evaporation of silicon phosphides and P₄ become the most considerable mechanisms of phosphorus evaporation at higher temperatures. However, the monoatomic evaporation of

phosphorus remains the main evaporation mechanism for P removal over the temperature range 1500 – 1820 °C, which is due to the high content of phosphorus in this sample. The industrial metallurgical grade silicon melts (feedstock for SoG – Si production) contain usually below 50 ppmw phosphorus [84], depending on the P content of the utilized raw materials. Hence, the results presented in Figure 10(a) will be of high interest for the vacuum refining of silicon in practice. These results reveal that the major part of P removal from silicon at ultra – high temperatures is by means of P₄ and silicon phosphides evaporation, while previously researchers only expected the monoatomic phosphorus evaporation and in some cases the diatomic phosphorus was considered for evaporation [85]. However, we showed that phosphorus can evaporate in the form of compounds like SiP, Si₂P, SiP₂ and Si₃P and the contribution of these species in P mass transport to gas phase is higher for lower phosphorus contents and higher temperatures.



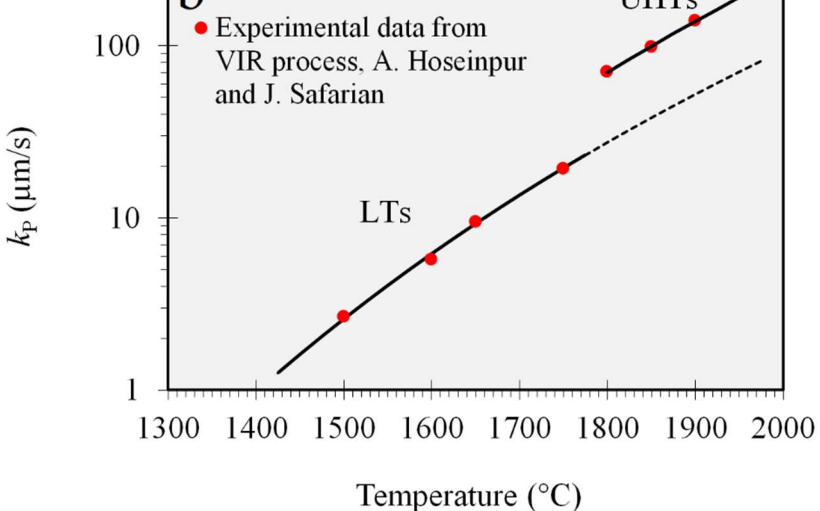


Figure 9.The changes of A_{t-P} with temperature for samples Si – 100 P and Si – 1250 P (a), and the change of k_P in vacuum induction refining of silicon by temperature (b); data from literature A.

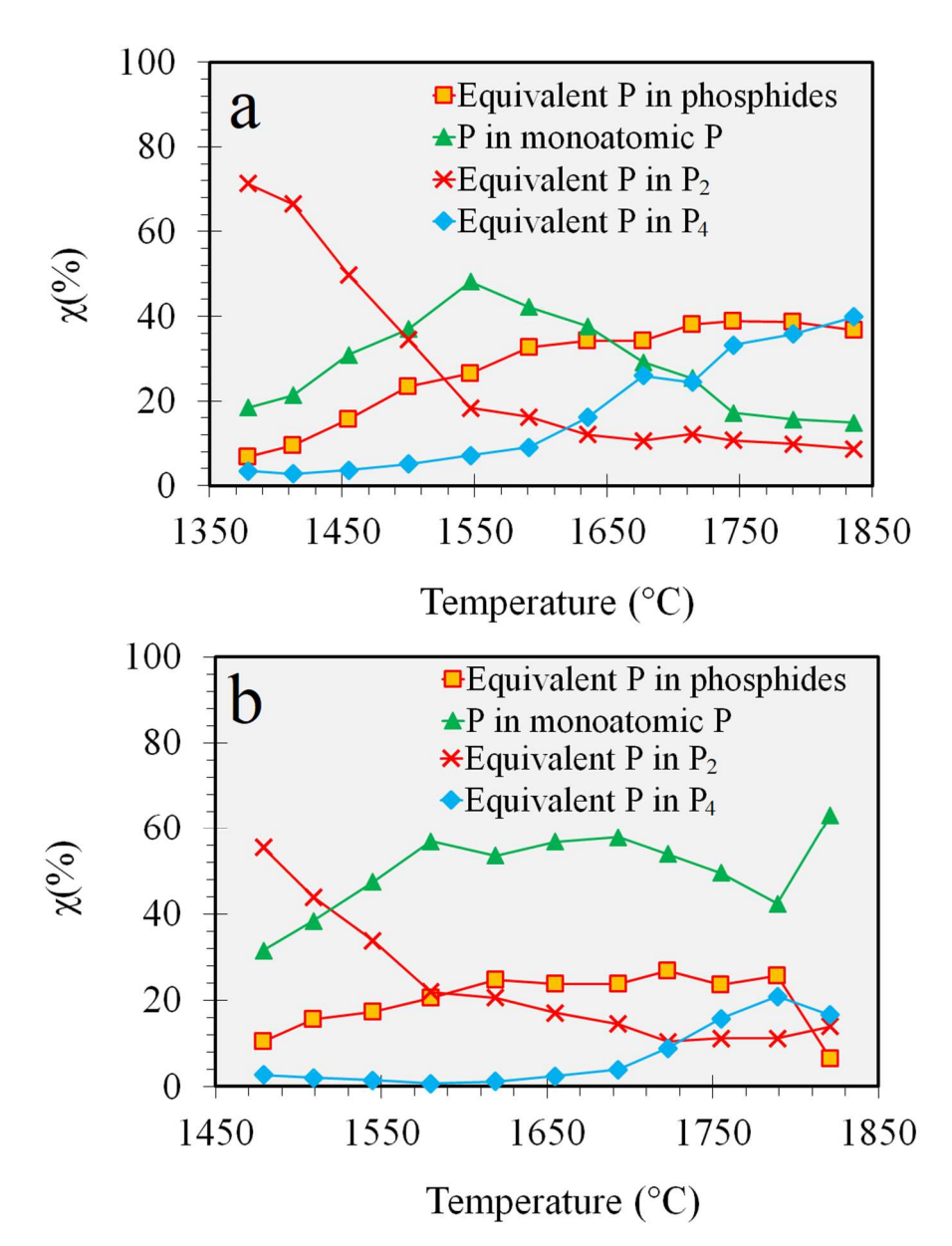


Figure 10. The evaporation impact χ_i of various phosphorus-containing species in evaporation of phosphorus from silicon, (a) Si – 100 P sample and (b): Si – 1250 P sample.

4.3 Mechanisms of P evaporation from liquid Si

According to literature, phosphorus evaporates from silicon melt in the forms of P and P_2 , as we also observed, and hence the only mechanism that could be assumed was the desorption of these species from the melt surface. This mechanism, however, cannot explain our silicon phosphides observations and the increase of the P removal from Si - P melt at ultra-high temperatures. On the other hand, when

dealing with the Si melts containing P, the high affinity of Si and P to each other should be respected. This makes the Si and P to establish strong covalent bonds and forming stable compounds like SiP, Si₂P, and SiP₂ in solid state. This strong affinity made it possible for the researchers to estimate the thermodynamic properties of Si – P system by theory of associated solutions. Hence, as mentioned by Zaitsev et al. ^[66], when dealing with Si – P melts, associative groupings of Si_xP_y are most probably possible. In other words, P can establish a covalent bond with the adjacent Si atom in the melt due to its high affinity to Si. Once that this bond is established between Si and P, forming a short-range order of Si and P atoms in the form of Si_xP_y, the thermodynamic properties of these groupings will be the same as the Si_xP_y compounds in solid state.

Previously, we proposed a hypothesis $^{[6]}$ about the decomposition of the transitional silicon phosphides (Si_xP_y) at the melt surface over the 1750 – 1800 °C, which could explain the jump in k_P (Fig 9b). According to this mechanism, the transferred phosphorus atoms from the bulk melt to the melt surface could be desorbed in the form of Si phosphides, especially at higher temperatures. We can discuss this hypothesis by studying the favorability for formation of Si_xP_y compounds at the melt surface. The only known condensed silicon phosphides are SiP and SiP₂ $^{[64,86]}$ and their thermodynamic data are available in HSC® software $^{[87]}$. The thermodynamic favorability for the formation of SiP and SiP₂ from dissolved phosphorus in liquid Si could be studied by the following reactions:

$$Si + \underline{P} = SiP_{(s)}, \Delta G^{\circ} = RTln(a_{P})$$
(8)

$$Si + 2\underline{P} = SiP_{2(s)}, \Delta G^{\circ} = 2RT \ln(a_{P})$$
(9)

Where $a_{\underline{P}}$ is the chemical activity of the dissolved phosphorus in silicon and could be calculated from the following relation:

$$a_P = \gamma_P^{\infty} x_P \tag{10}$$

Where $\gamma_{\underline{P}}^{\infty}$ is the activity coefficient of phosphorus in infinitely dilute solutions of phosphorus in silicon, and is already obtained by Zaitsev et.al. [66] in Table 4. The ΔG° values for the above reactions are calculated and presented in Figure 11. From this figure it is obvious that the formation of SiP and SiP₂ compounds from the dissolved phosphorus in liquid Si are thermodynamically feasible, and hence they can be formed and then evaporated. Moreover, this figure indicates that with the decrease of the phosphorus content in the melt, the formation of SiP and SiP₂ becomes thermodynamically more favorable. We assumed several decomposition routes for these phosphides, as they are all presented on Figure 12 together with the calculated ΔG° values. Figure 12 indicates that the ΔG° for reaction (e) shifts to negative values over temperature range of 1560 – 1600 °C, which leads to produce P₄. This

is in good agreement with KEMS results presented in Figure 6 where we showed the P_4 intensity increases by hitting this temperature range. In addition, the ΔG° for the reactions (a) to (d) shift to negatives values beyond 1750 °C which could explain observing the increase in A_{t-P} in KEMS trials at high temperatures.

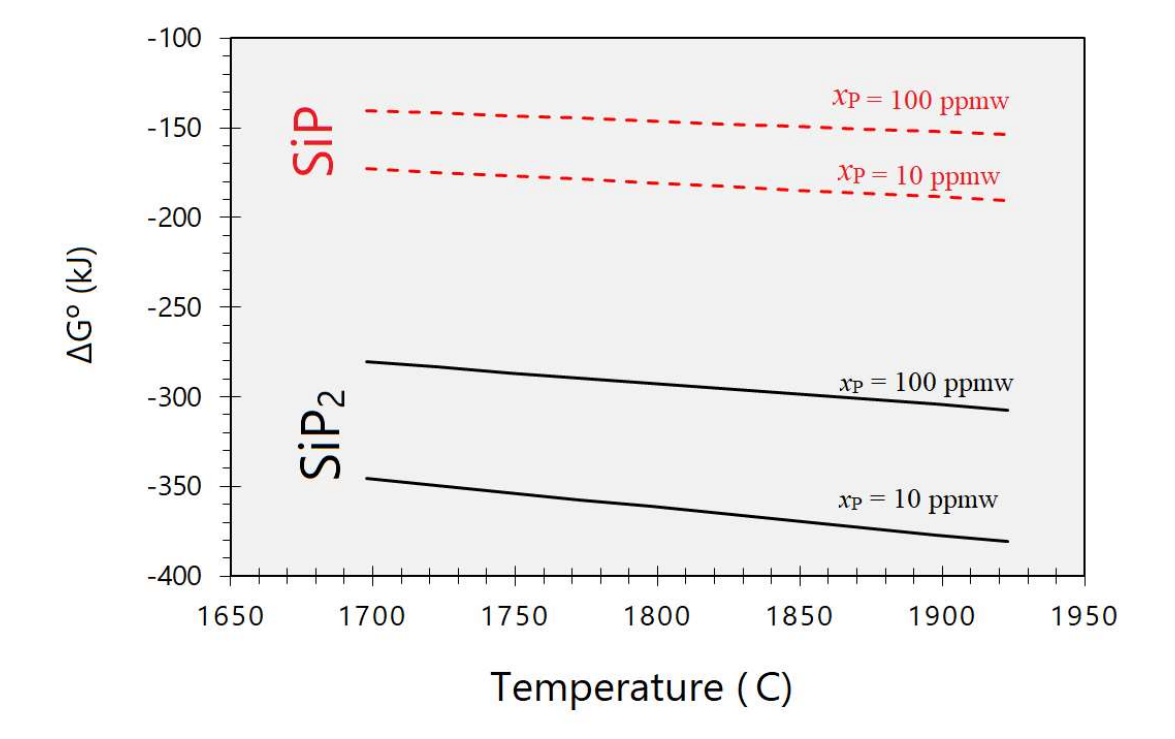


Figure 11. The Gibbs energy changes for the formation of condensed SiP and SiP₂ from the dissolved phosphorus in liquid silicon.

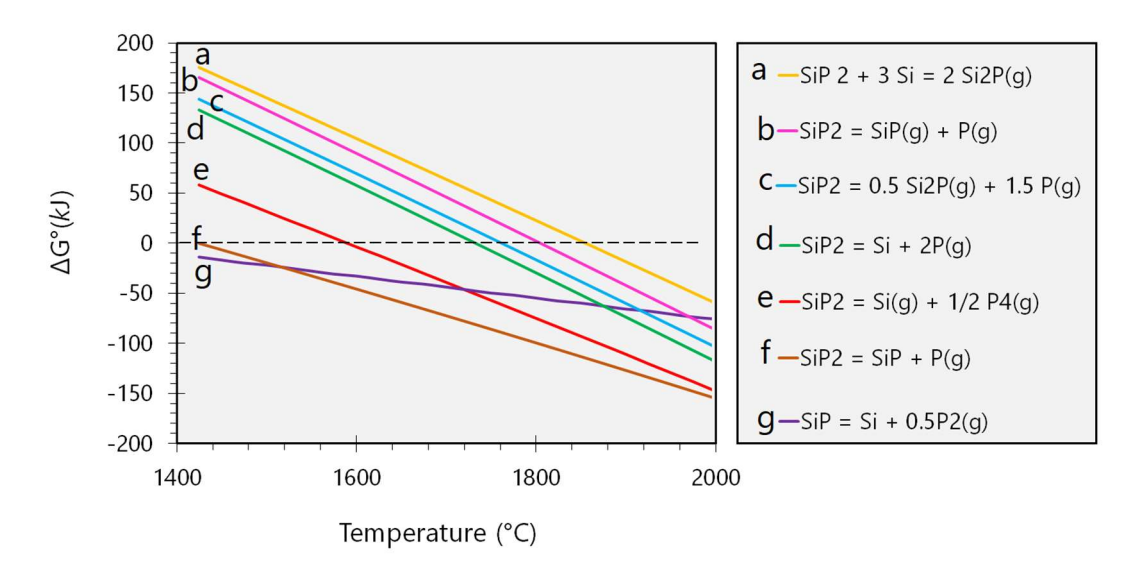


Figure 12. The Gibbs energy changes for different decomposition reactions of SiP and SiP₂.

In polythermal KEMS experiments, we observed more formation of P_4 beyond 1550 °C, a significant increase in the I_{t-P} beyond 1750 °C (Figure 9), and the detection of various silicon phosphides. These can be explained by the possible decomposition of transient silicon phosphides at the melt surface. Hence, we can introduce three main groups of reactions leading to phosphorus evaporation from the melt surface, as follows;

1. Molecular evaporation: formation and desorption of phosphorus species (P, P₂, and P₄) at the melt surface.

2. Decomposition of transient silicon phosphides: in this mechanism the transient silicon phosphides are decomposed to phosphorus species (P, P₂, and P₄) and other lower phosphides (Si_xP_y).

3. Evaporation of lower silicon phosphides (formed in mechanism 2) formed at the melt surface: in this mechanism the transient silicon phosphides could directly desorb at the melt surface.

Here it is worth mentioning that the monoatomic phosphorus desorption from melt surface is reasonably assumable since it only requires a single atom that has already reached to the melt surface to be desorbed. However, when it comes to the P_2 and P_4 formation and desorption, it requires two and four phosphorus atoms to join at the melt surface, respectively. Therefore, from a statistic point of view the formation of P_2 and P_4 molecules and their desorption from the melt surface is less feasible as there are only a few or tens of P_4 atoms per one million atoms of P_4 in the liquid phase.

Hence, mechanism (1) via P₂ and P₄ formation and desorption is important at higher P

concentrations, and for the very dilute solutions they are most likely formed via joining of P atoms over the surface. Obviously, in mechanism (1) we may consider that there is not significant interaction between the P and Si atoms. However, another mechanism may be the formation of a sort of bonding between the P and Si atoms at the melt surface, yielding Si_xP_y molecules, depending on the P concentration. This hypothesis is logical since we observed higher intensities of SiP species than SiP₂ by KEMS as it could be a product for the decomposition of SiP₂. If Si_xP_y molecules are formed, which is more favorable at lower P concentrations and higher temperatures, they will then contribute via mechanisms (2) and (3) in the P mass transport. Our results may suggest that at low temperatures these Si_xP_y molecules are more decomposed to P, P₂, and P₄ species, and with increasing temperature mechanism (3) becomes more important, particularly above 1750 °C. The above mechanisms for phosphorus evaporation are schematically shown in Figure (13), indicating on the important role of melt surface in phosphorus evaporation from liquid Si.

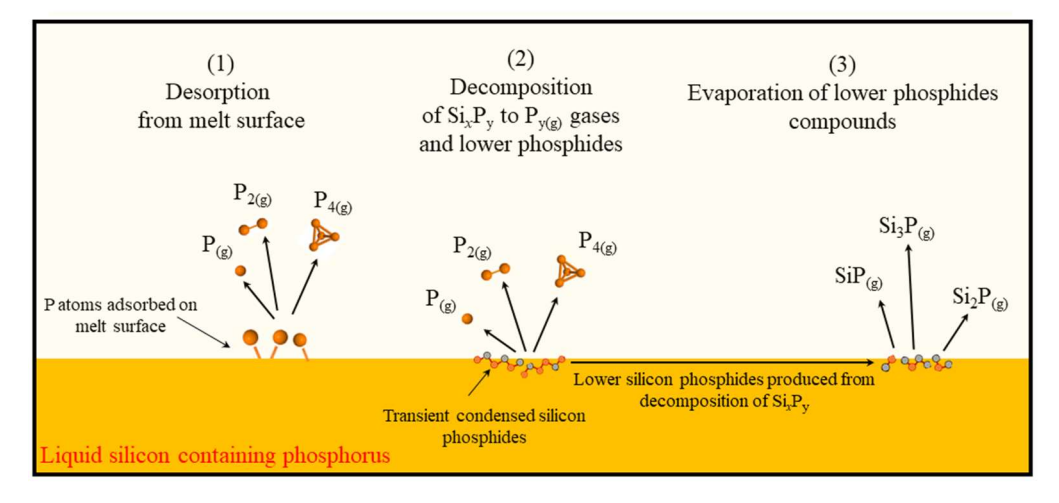


Figure 13. A schematic representation indicating three routes for phosphorus evaporation from silicon melt surface.

5 Conclusions

Vacuum evaporation of phosphorus from liquid silicon was experimentally investigated by KEMS. The following remarks should be highlighted as the outcomes of this research:

- 1. Various phosphorus compounds were experimentally detected by KEMS: P and P₂ (detected before in literature) and the new P₃, P₄, SiP, Si₂P, Si₃P, and SiP₂ species.
- 2. The overall evaporation rate of phosphorus species is intensified at ultra-high temperatures, above 1650 °C, which agrees well with the previous results about vacuum refining of silicon.

- 3. It was found that up to about 40 % of the evaporation could be by means of molecular silicon phosphides evaporation, when initial P content < 100 ppmw and T > 1750 °C.
- 4. It was found that the evaporation of P₄ molecules becomes considerable beyond 1550°C and
 up to 40 % of phosphorus removal could be by means of P₄ evaporation at ultra high
 temperatures (T_{UHT} ≥ 1.25 T_{m, Si}).
- 5. The relationship between the vapor pressure of the phosphorus species (P, P₂, P₄, SiP, Si₂P) and their concentrations in liquid Si at 1442 °C were determined.

649

650

Acknowledgments

References

- This research was financed by Norwegian University of Science and Technology (NTNU) and was
- done in cooperation with Jülich research center, in Jülich, Germany. The authors are thankful to Dr.
- Elena Yazhenskikh from Jülich Forschungszentrum for her comments about FactSage databases and
- Dr. Lars Klemet Jakobsson from Elkem in Kristiansand for his comments on the manuscript.

655

656

Conflict of interest statement

On behalf of all authors, the corresponding author states that there is no conflict of interest.

658659

- Forniés, Ceccaroli, Méndez, Souto, Pérez Vázquez, Vlasenko, and Dieguez: *Energies*, 2019, vol. 12, p. 1495.
- S. Zheng, J. Safarian, S. Seok, S. Kim, T. Merete, and X. Luo: *Trans. Nonferrous Met. Soc. China*, 2011, vol. 21, pp. 697–702.
- 665 3 T. Kemmotsu, T. Nagai, and M. Maeda: High Temp. Mater. Process., 2011, vol. 30, pp. 17–22.
- 666 4 S. Shi, P. Li, J. Meng, D. Jiang, Y. Tan, and H.M.N. ul H.K. Asghar: *Phys. Chem. Chem. Phys.*, 2017, vol. 19, pp. 28424–33.
- 668 5 S.M. Karabanov, D. V. Suvorov, D.Y. Tarabrin, E. V. Slivkin, A.E. Serebryakov, V. V. Klimakov,
- A.S. Karabanov, and O.A. Belyakov: in 2019 IEEE International Conference on Environment and
- 670 Electrical Engineering and 2019 IEEE Industrial and Commercial Power Systems Europe (EEEIC /
- 671 *I&CPS Europe*), IEEE, 2019, pp. 1–5.
- 672 6 A. Hoseinpur and J. Safarian: *Vacuum*, 2021, vol. 184, p. 109924.
- 673 7 A. Hoseinpur and J. Safarian: *Vacuum*, 2020, vol. 171, p. 108993.
- 674 8 M. Zhu, A. Azarov, E. Monakhov, K. Tang, and J. Safarian: Sep. Purif. Technol., 2020, vol. 240, p.
- 675 116614.
- 676 9 A. Hosseinpour and L. Tafaghodi Khajavi: Metall. Mater. Trans. B, 2019, vol. 50, pp. 1773–81.
- 677 10 L.T. Khajavi, K. Morita, T. Yoshikawa, and M. Barati: *J. Alloys Compd.*, 2015, vol. 619, pp. 634–8.

- 678 11 L.T. Khajavi, K. Morita, T. Yoshikawa, and M. Barati: Metall. Mater. Trans. B Process Metall. Mater.
- 679 *Process. Sci.*, 2014, vol. 46, pp. 615–20.
- 680 12 L.T. Khajavi, K. Morita, T. Yoshikawa, and M. Barati: *J. Alloys Compd.*, 2015, vol. 619, pp. 634–8.
- A. Hoseinpur, S. Andersson, K. Tang, and J. Safarian: Langmuir, 2021, vol. 37, pp. 7473–85.
- A. Hoseinpur and J. Safarian: in 35th European Photovoltaic Solar Energy Conference and Exhibition
- 683 *Phosphorus*, Bruxel, 2018, pp. 469–72.
- A. Hosseinpour and L. Tafaghodi Khajavi: Miner. Process. Extr. Metall. Rev., 2018, vol. 39, pp. 308–
- 685 18.
- 686 16 C. Battaglia, A. Cuevas, and S. De Wolf: *Energy Environ. Sci.*, 2016, vol. 9, pp. 1552–76.
- 687 17 Shell Scenarios: Sky Meeting the Goals of the Paris Agreement, 2018.
- 688 18 IRENA: Future of Solar Photovoltaic: Deployment, Investment, Technology, Grid Integration and
- Socio-Economic Aspects, 2019.
- 690 19 A. Jäger-Waldau: PV Status Report 2019, Luxembourg, 2019.
- 691 20 S. Meyer, S. Wahl, A. Molchanov, K. Neckermann, C. Möller, K. Lauer, and C. Hagendorf: Sol.
- 692 Energy Mater. Sol. Cells, 2014, vol. 130, pp. 668–72.
- 693 21 G.M. Wilson, M. Al-Jassim, W.K. Metzger, S.W. Glunz, P. Verlinden, G. Xiong, L.M. Mansfield, B.J.
- 694 Stanbery, K. Zhu, Y. Yan, J.J. Berry, A.J. Ptak, F. Dimroth, B.M. Kayes, A.C. Tamboli, R. Peibst, K.
- 695 Catchpole, M.O. Reese, C.S. Klinga, P. Denholm, M. Morjaria, M.G. Deceglie, J.M. Freeman, M.A.
- Mikofski, D.C. Jordan, G. TamizhMani, and D.B. Sulas-Kern: J. Phys. D. Appl. Phys., 2020, vol. 53,
- 697 p. 493001.
- 698 22 M. Zhu, A. Azarov, E. Monakhov, K. Tang, and J. Safarian: Sep. Purif. Technol., 2020, vol. 240, p.
- 699 116614.
- 700 23 L. Sun, Z. Wang, H. Chen, D. Wang, and G. Qian: Metall. Mater. Trans. B, 2017, vol. 48, pp. 420–8.
- 701 24 Y. Li and J. Chen: *Met. Mater. Int.*, 2020, vol. 26, pp. 526–31.
- 702 25 C. Zhang, H. Lai, Y. Zhang, Z. Sheng, J. Li, P. Xing, and X. Luo: Sep. Purif. Technol., 2020, vol. 232,
- 703 p. 115954.
- A. Hosseinpour and L. Tafaghodi Khajavi: Metall. Mater. Trans. B, 2019, vol. 50, pp. 1773–81.
- 705 27 D. Jiang, S. Ren, S. Shi, W. Dong, J. Qiu, Y. TAN, and J. Li: *J. Electron. Mater.*, 2014, vol. 43, pp.
- 706 314–9.
- J. Li, H. Tang, Z. Guo, and Y. Lin: in 2013 International Conference on Materials for Renewable
- 708 *Energy and Environment*, vol. 1, IEEE, 2013, pp. 17–20.
- 709 29 L.T. Khajavi and M. Barati: *High Temp. Mater. Process.*, 2012, vol. 31, pp. 627–31.
- 710 30 S. Shi, P. Li, Z. Sheng, D. Jiang, Y. Tan, D. Wang, S. Wen, and H.M.N. ul H.K. Asghar: *Energy*,
- 711 2019, vol. 185, pp. 102–10.
- 712 31 S.M. Karabanov, D. V. Suvorov, D.Y. Tarabrin, E. V. Slivkin, A.E. Serebryakov, V. V. Klimakov,
- 713 A.S. Karabanov, and O.A. Belyakov: in AIP Conference Proceedings, vol. 1999, 2018, p. 020012.
- J.K. Lee, J.S. Lee, B.Y. Jang, J.S. Kim, Y.S. Ahn, G.H. Kang, H.E. Song, M.G. Kang, and C.H. Cho:
- 715 Sol. Energy, 2015, vol. 115, pp. 322–8.
- 716 33 J. Safarian, K. Tang, and K. Hildal: in 2015 sustainable industrial processing summit, vol. 3, 2015, pp.
- 717 261–8.

- 718 34 A. Hoseinpur, G. Tranell, and J. Safarian: in *silcion for the chemical and solar industry XV*, 2020, pp.
- 719 261–72.
- 720 35 C. Gan, S. Wen, Y. Liu, W. Wen, J. Chen, and X. Luo: *Int. J. Therm. Sci.*, 2021, vol. 159, p. 106615.
- 721 36 S.M. Karabanov, D. V. Suvorov, D.Y. Tarabrin, E. V. Slivkin, A.S. Karabanov, O.A. Belyakov, A.A.
- 722 Trubitsyn, and A. Serebryakov: *MRS Adv.*, 2019, vol. 4, pp. 1937–47.
- 723 37 E. Forines, A. Souto, T. Velasenko, A. Perez Vazquez, M. Tojeiro, M. Anoshenko, and G. Varela: in
- 35th European Photovoltaic Solar Energy Conference and Exhibition PERFORMANCE, 2018, pp.
- 725 473–5.
- 726 38 L. Huang, H. Lai, C. Lu, M. Fang, W. Ma, P. Xing, X. Luo, and J. Li: J. Electron. Mater., 2016, vol.
- 727 45, pp. 541–52.
- 728 39 S. Qiu, S. Ren, L. Huang, T. Tang, M. Fang, and X. Luo: *Vacuum*, 2016, vol. 128, pp. 66–72.
- 729 40 D. Jiang, S. Shi, S. Ren, H.M.N. ul H. Khan Asghar, Y. Tan, P. Li, J. Qiu, and J. Li: Renew. Energy,
- 730 2015, vol. 77, pp. 463–6.
- 731 41 A. Hoseinpur, K. Tang, and J. Safarian: Sep. Purif. Technol., 2020, vol. 235, p. 116284.
- 732 42 J. Safarian and M. Tangstad: High Temp. Mater. Process., 2012, vol. 31, pp. 73–81.
- 733 43 J. Safarian and M. Tangstad: *Metall. Mater. Trans. B*, 2012, vol. 43, pp. 1427–45.
- 734 44 J.M. Souto, Alejandro; Bullón, Javier; Ordás, Ramón; Míguez: Proc. Silicon Chem. Sol. Ind. XII,
- 735 2014, pp. 67–76.
- 736 45 I. Langmuir: J. Am. Chem. Soc., 1932, vol. 54, pp. 2798–832.
- 737 46 R.G. Remorov and M.W. Bardwell: *Surf. Sci.*, 2005, vol. 585, pp. 59–65.
- 738 47 K.L. Walter: Iowa State University, Digital Repository, 1972.
- 739 48 E. Bird and Z. Liang: *Phys. Rev. E*, 2020, vol. 102, p. 043102.
- 740 49 W. Steckelmacher: *Reports Prog. Phys.*, 1986, vol. 49, pp. 1083–107.
- 741 50 K. Hilpert: 1990, pp. 97–198.
- L. Bencze, M. Rys-Matejczuk, E. Yazhenskikh, M. Ziegner, and M. Müller: *Energy and Fuels*, 2016,
- 743 vol. 30, pp. 657–65.
- N.S. Jacobson and B.A. Kowalski: *Thermodynamic Measurements Using the Knudsen Cell Technique*,
- 745 Ohio, 2020.
- 746 53 J. Drowart, C. Chatillon, J. Hastie, and D. Bonnell: *Pure Appl. Chem.*, 2005, vol. 77, pp. 683–737.
- J. Drowart: in Mass Spectrom., Proc. Int. Sch. Mass Spectrom., Ljubliana, 1971, pp. 187–242.
- 748 55 Z.H. Dong, D. Sergeev, D. Kobertz, N. D'Souza, S. Feng, M. Müller, and H.B. Dong: *Metall. Mater*.
- 749 Trans. A Phys. Metall. Mater. Sci., 2020, vol. 51, pp. 309–22.
- 750 56 S. Fürtauer and H. Flandorfer: *J. Alloys Compd.*, 2019, vol. 781, pp. 1110–8.
- 751 57 E.N. Kablov, V.L. Stolyarova, V.A. Vorozhtcov, S.I. Lopatin, and F.N. Karachevtsev: J. Alloys
- 752 *Compd.*, 2019, vol. 794, pp. 606–14.
- 753 58 O.Y. Kurapova, S.M. Shugurov, E.A. Vasil'eva, V.G. Konakov, and S.I. Lopatin: *J. Alloys Compd.*,
- 754 2019, vol. 776, pp. 194–201.
- 755 59 D. Sergeev, E. Yazhenskikh, D. Kobertz, and M. Müller: Calphad Comput. Coupling Phase Diagrams
- 756 *Thermochem.*, 2019, vol. 65, pp. 42–9.
- 757 60 C.M. Arvhult, C. Guéneau, S. Gossé, and M. Selleby: *J. Alloys Compd.*, 2018, vol. 767, pp. 883–93.

- 758 61 V.A. Vorozhtcov, V.L. Stolyarova, S.I. Lopatin, E.P. Simonenko, N.P. Simonenko, K.A. Sakharov,
- 759 V.G. Sevastyanov, and N.T. Kuznetsov: *J. Alloys Compd.*, 2018, vol. 735, pp. 2348–55.
- 760 62 Y. Wang, P. Zhou, Y. Peng, Y. Du, B. Sundman, J. Long, T. Xu, and Z. Zhang: J. Alloys Compd.,
- 761 2016, vol. 687, pp. 855–66.
- D. Henriques, V. Motalov, L. Bencze, S. Fürtauer, H. Flandorfer, and T. Markus: J. Alloys Compd.,
- 763 2016, vol. 687, pp. 306–11.
- 764 64 S.-M. Liang and R. Schmid-Fetzer: J. Phase Equilibria Diffus., 2014, vol. 35, pp. 24–35.
- 765 65 T. Miki, K. Morita, and N. Sano: *Metall. Mater. Trans. B*, 1996, vol. 27, pp. 937–41.
- 766 66 A.I. Zaitsev, A.D. Litvina, and N.E. Shelkova: *High Temp.*, 2001, vol. 39, pp. 227–32.
- 767 S. Favre, I. Nuta, G. Chichignoud, K. Zaïdat, and C. Chatillon: ECS J. Solid State Sci. Technol., 2016,
- 768 vol. 5, pp. P129–37.
- J. Safarian, K. Tang, K. Hildal, and G. Tranell: *Metall. Mater. Trans. E*, 2014, vol. 1, pp. 41–7.
- 770 69 S.S. Zheng, W.H. Chen, J. Cai, J.T. Li, C. Chen, and X.T. Luo: Metall. Mater. Trans. B Process
- 771 *Metall. Mater. Process. Sci.*, 2010, vol. 41, pp. 1268–73.
- 772 70 S.S. Zheng, T. Abel Engh, M. Tangstad, and X.T. Luo: Sep. Purif. Technol., 2011, vol. 82, pp. 128–37.
- 773 71 T. Ikeda and M. Maeda: ISIJ Int., 1992, vol. 32, pp. 635–42.
- 774 72 S. Shi, W. Dong, X. Peng, D. Jiang, and Y. Tan: *Appl. Surf. Sci.*, 2013, vol. 266, pp. 344–9.
- 775 73 K. Suzuki, K. Sakaguchi, T. Nakagiri, and N. Sano: *J. Japan Inst. Met.*, 1990, vol. 54, pp. 161–7.
- 776 74 M.E. Schlesinger: Chem. Rev., 2002, vol. 102, pp. 4267–302.
- 777 75 J. Safarian and M. Tangstad: *J. Mater. Res.*, 2011, vol. 26, pp. 1494–503.
- 778 76 L.S. Kudin, M.F. Butman, D.N. Sergeev, V.B. Motalov, and K.W. Krämer: J. Chem. Eng. Data, 2012,
- 779 vol. 57, pp. 436–8.
- 780 77 J.B. Mann: in *Proceedings of the Conference on Mass Spectrometry*, K. Ogata and T. Hayakawa, eds.,
- 781 University Park Press, Baltimore, 1970, pp. 814–9.
- 782 V.P. Glushko: Thermodynamic Properties of Individual Substances, 1st edn., Nauka, Moscow, 1982.
- 783 79 D. Spathara, D. Sergeev, D. Kobertz, M. Müller, D. Putman, and N. Warnken: J. Alloys Compd., 2021,
- 784 vol. 870, p. 159295.
- 785 80 T. Tomooka, Y. Shoji, and T. Matsui: *J. Mass Spectrom. Soc. Jpn.*, 1999, vol. 47, pp. 49–53.
- 786 81 O. Kubachewski and C.B. Alcock: Metallurgical Thermochemistry, 5th edn., Pergamon press ltd,
- 787 NewYork, 1979.
- 788 82 C.W. Bale, E. Bélisle, P. Chartrand, S.A. Decterov, G. Eriksson, A.E. Gheribi, K. Hack, I.H. Jung,
- 789 Y.B. Kang, J. Melançon, A.D. Pelton, S. Petersen, C. Robelin, J. Sangster, P. Spencer, and M.A. Van
- 790 Ende: Calphad Comput. Coupling Phase Diagrams Thermochem., 2016, vol. 54, pp. 35–53.
- 791 83 Factsage software version 7.3, www.factsage.com.
- 792 84 M. Zhu, A. Azarov, E. Monakhov, K. Tang, and J. Safarian: Sep. Purif. Technol., 2020, vol. 240, p.
- 793 116614.
- 794 85 S. Zheng, T.A. Engh, M. Tangstad, and X.-T. Luo: *Metall. Mater. Trans. A*, 2011, vol. 42, pp. 2214–
- 795 25.
- 796 86 H.T. Kwon, C.K. Lee, K.J. Jeon, and C.M. Park: *ACS Nano*, 2016, vol. 10, pp. 5701–9.
- 797 87 HSC chemistry 10, http://www.hsc-chemistry.net/index.html.

801 Graphical abstract

